A NEW METHOD OF SEISMIC RETROFITTING COST ANALYSIS AND EFFECTIVENESS FOR REINFORCED CONCRETE STRUCTURES

George Markou

Department of Civil Engineering, University of Pretoria, Hatfield Campus, South Africa

e-mail: george.markou@up.ac.za

Highlights

- Cyclic nonlinear analyses are performed through 3D detailed models on full-scale RC structures.
- In depth analysis of the seismic performance of CFRP sheet retrofitted RC structures.
- In depth analysis of the seismic performance of infill RC shear wall retrofitted RC structures.
- A new optimum retrofitting cost effectiveness factor is proposed.
- A cost effectiveness analysis on the retrofitting strategies is presented.

Abstract

Modeling, analysis and design of retrofitting interventions has been a topic of numerous research projects that aim in providing answers to complex questions such as "which retrofitting technique is more effective in terms of cost and frame mechanical enhancement?", and "what is the overall strength enhancement in terms of structural seismic performance?" Therefore, a main purpose of this manuscript is to support decision-making, thus providing a numerical method that can be used to select the optimum retrofit strategy based on the mechanical response of reinforced concrete (RC) structures. The currently available numerical tools for the 3D detailed mechanical limit state study of the structural behavior of retrofitted RC elements are currently bound by numerous numerical and computational constraints, thus are usually implemented at the level of a single structural member under nonlinear or elastic monotonic loading. This work alleviates these constraints through the use of the hybrid modeling (HYMOD) approach [1-3] which is used to develop a finite element model that is numerically validated through the use of a full-scale multistorey RC building that was retrofitted with infill RC walls and carbon fibre reinforced polymer (CFRP) jacketing. Further validation was

also performed and presented in this manuscript on joints that foresaw the use of 3 layers of CFRP sheets. The understudy 4-storey RC building, which was experimentally tested under ultimate limit state cyclic loading, was used to develop 24 models that foresaw different retrofitting strategies. Two retrofitting techniques were investigated herein, the CFRP jacketing and the infill RC shear walls, where for the case of the later four different rebar materials were investigated (Steel-, Glass-, Aramid- and Carbon-FRP). In order to determine the optimum cost-effectiveness of each strengthening intervention, an optimum retrofitting cost-effectiveness factor is proposed that takes into account the overall cost of the retrofitting strategy in relation to the respective strength and energy dissipation enhancement that is achieved compared to the initial bare RC frame. Based on the proposed factor and the numerical findings during the seismic assessment of the understudy retrofitting strategies, it was concluded that the use of infill RC shear walls with Aramid-FRP rebars was the most cost-effective strengthening method when both strength and energy dissipation enhancement was within the desired design. For the case where the main objective was the increase of strength (base shear) the use of infill RC shear walls with CFRP rebars was found to be the most cost-effective option. Furthermore, when comparing standard steel-reinforced shear walls with CFRP jacketing, the use of CFRP sheets was found to be more cost-effective in the case where strength enhancement was the main objective. According to the numerical investigation performed herein, more numerical investigation is deemed necessary for the study of the cost-effectiveness of more strengthening methods and seismic isolation systems, where more RC structures and bridges will also be considered.

Keywords: Retrofitting Design, Cost optimization, CFRP Jacketing, Infill RC shear walls, G-A-CFRP rebars, Nonlinear Cyclic Loading.

1. Introduction

Over the last few decades, the civil engineering industry has used three main retrofitting techniques for strengthening the framing systems of RC buildings. Namely these methods are:

i. CFRP jacketing,

ii. RC jacketing and

iii. Infill RC shear walls.

Determining the final strength of a retrofitted RC section through numerical or analytical tools has been a great challenge for the international scientific community given the complexity of the problem. From the design code point of view, the most comprehensive attempt to provide with methodologies and corresponding formulae in order to address this issue, was the Greek code for structural interventions (ΚΑΝΕΠΕ [4]), which comprises of approximately 350 pages of recommendations and it is also in line with the Eurocode 8 provisions [5] for designing earthquake resistant structures. The Greek structural interventions code mainly provides semi-empirical formulae and recommendations in regards to the strengthening of single structural members according to the adopted retrofitting method, while suggesting general guidelines when it comes to the checks that are required to be performed at a building level and general suggestions related to modeling with the finite element (FE) method. Therefore, the need for a numerical method that will provide the ability to objectively model and analyse the nonlinear mechanical behavior of retrofitted RC buildings is of great importance.

When designing the strengthening interventions of a RC building, the formulae used in order to compute the final capacity of strengthened members [4] foresee simplification assumptions that eventually derive a final design that does not represent the actual mechanical response of the structure. The complexity of the at hand task directly derives from the nature of the problem that simultaneously deals with two complicated mechanical problems; the first is that of the accurate prediction of the existing member's resistance and the capacity of the strengthening intervention alone, while the second is to compute the enhanced overall strength of the retrofitted structural member by accounting the interaction between the two domains (existing and new materials). In addition to that, the computation of the overall mechanical behavior of the structure (which is significantly affected by the strengthening strategy) by accounting for a detailed numerical method that will foresee an accurate nonlinear cyclic simulation of all strengthened members, is still not available given the computational demands that rise when using 3D detailed modeling approaches [6, 7].

Numerous research publications can be found in the international literature related to the use of the 3D detailed modeling approach that foresees the discretization of the concrete domain through the use of solid elements and perform an exact discretization of the rebars through rod or beam FEs. The retrofitting intervention, in the case of CFRP jacketing, is modelled through the use of hexahedral or shell FEs. The first FE modeling attempt of RC FRP strengthened beams was published by Arduini et al. [8] in 1997. Finite Element Analysis (FEA) with the smeared crack approach was used to simulate the behavior and failure mechanisms of FRP composite RC beams. In addition to this research work, an FRP-strengthened RC bridge was modelled through FEs [9], where truss elements were used to simulate the mechanical behavior of the FRP composites.

Kachlakev et al. [10] discussed the use of 3D detailed modeling in RC strengthening cases of single membered structures and a part of a small RC bridge that were modelled under monotonic loading. In their report, they used linear and nonlinear FE models that had been strengthened with FRP composites through the use of ANSYS [11] and SAP2000 [12]. The use of 8-noded hexahedral elements was adopted so as to discretize the concrete medium, where the cracking was modelled through the smeared crack approach [13]. In order to numerically model the FRP jackets, the layered solid element was used. Due to computational restraints, they had to model a quarter of the beam specimens that were studied by taking advantage of the symmetry of the strengthened beam geometry.

The same modeling approach described in [10] was adopted by Mostofinejad and Talaeitaba [14], where they numerically simulated an external RC joint that was strengthened with FRP composites. The modeling performed in this work foresaw monotonic nonlinear analyses that were compared with experimental data. Godat et al. [15] numerically investigated the mechanical behavior of shear reinforced beams that foresaw the use of side-bonded FRP sheets, U-wrap FRP strengthening configurations and anchored FRP sheets. For the 3D detailed modeling needs of their work, the commercial software ADINA [16] was used, where a comparison between the numerical predictions and test results was performed in order to validate the developed models that were analysed under nonlinear monotonic loading conditions. As reported in their work, the developed models managed to capture the experimental results, while the strengthening with U-shaped strips led to the lowest

amounts of interfacial slip. Koteš and Kotula [17] modelled RC girders with T-shaped sections through the use of 2D and 3D models that were developed in ATENA software [18]. The strengthening method that was modelled in their work, was that of CFRP laminates that were installed at the bottom of the T-section and assumed to be fully bonded with the concrete medium. The monotonic nonlinear analyses that were performed, showed a good agreement with the experimental data as reported by the authors [17].

Ibrahim and Mahmood [19] presented an analysis model for RC beams externally reinforced with FRP laminates. Their model was developed in ANSYS [11] and the assumptions for developing the FE models followed the same simulation concept that was recommended in [10]. The bond assumption assumed no-slip considerations, while the monotonic nonlinear analysis showed a good agreement with the experimental results. A basic conclusion from this research work was that CFRP retrofitting was found to be more efficient than Glass-FRP (GFRP) for shear strengthening. Chansawat et al. [20] extended the work that was presented in [10] through the same modeling approach so as to simulate the behavior of full-scale RC beams strengthened with G- and C-FRP sheets. Their findings indicated that the proposed 3D model was able to conservatively capture the failure load of the strengthened beams under monotonic nonlinear loading conditions.

Another research work that also used the ANSYS software to model CFRP retrofitted exterior and interior joints, was presented by Niroomandi et al. [21]. The numerical findings of this work indicated a significant increase of the carrying capacity of the retrofitted joints. Young-Min et al. [22] performed nonlinear FE analysis in order to investigate the structural response of prestressed RC beams strengthened with CFRP in shear. For the construction of their models, which were analysed under monotonic loading, they used DIANA [23] commercial software that incorporates the smeared crack approach, whereas the concrete was assumed to have a softening branch. Based on the published force vs displacement curves, the numerical results are in a good agreement with the experimental data up to the level of the maximum force capacity, while the numerical predictions seem to overestimate in almost all cases the ultimate displacement. This is most probably attributed to the use of the softening branch when simulating the mechanical response of concrete that foresees a numerical behavior that

derives an additional ductility.

Sinaei et al. [24] and Shurai [25] published work on modeling of CFRP retrofitted joints and beams, respectively, through the use of 3D analyses with hexahedral elements incorporated within the commercial software ABAQUS [26]. Both studies used experimental results to compare the numerical response of their models, where they reported a good agreement between the numerical and experimental push-over curves. El-Hacha et al. [27] chose to numerically investigate the mechanical behavior of a composite beam (steel I-beam with a RC flange) that was strengthened with a CFRP plate at the bottom flange. In their study, the commercial software ANSYS was used, while the under-study specimen was discretized with 12,510 elements and was validated through experimental data. The analysis foresaw the execution of monotonic nonlinear analyses, which demonstrated a good agreement with the experimental results. This approach was found to be accurate but hindered by excessive computational cost (given the significantly large number of solid elements used to discretize the beam), hence makes it practically not feasible to apply this approach for the study of full-scale structures.

One of the very few research works found in the international literature that deals with cyclic loading and CFRP retrofitting is that of Cortés-Puentes and Palermo [28], who studied the behavior of RC shear walls strengthened by using different configurations. In order to perform their numerical analyses, they used VecTor2, which is a 2D finite element software. The obtained numerical results illustrated the ability to capture the hysteretic loops that resulted from the experimental tests. Nevertheless, the applicability of this modeling approach is limited geometrically to 2D problems. The same year (2012) Alhaddad et al. [29] published a work related to the 3D detailed modeling of RC exterior beam-column joints strengthened with CFRP sheets through ANSYS. The analyses that were performed foresaw monotonic nonlinear loading conditions, while the numerically obtained results were compared with the experimental envelope curves (given that the experimental setups foresaw the cyclic loading of the RC retrofitted specimens). One of the main findings in this work was that the CFRP sheet strengthening outperformed the corresponding GFRP in terms of strength enhancement.

LS-DYNA [30] commercial software was used by Elsanadedy et al. [31] for the numerical simulation of FRP-wrapped concrete columns under monotonic loading, while the same software was used in Elsanadedy et al. [32], where the experimental and numerical investigation were presented on the flexural strengthening of RC beams using textile reinforced mortar. The adopted approach foresaw the use of hexahedral elements so as to discretize both textile reinforced mortar and concrete domains, where the models were tested under monotonic loading. Milani and Lourenço [33] presented a numerical investigation on a simple model for the monotonic nonlinear analysis of FRP-strengthened masonry structures, where they developed their 3D models by using DIANA [23] commercial software. Based on their numerical findings, their proposed model managed to efficiently capture the experimental data.

Another research work that used ANSYS commercial software was published by Anania and D'Agata [34], where a small CFRP strengthened RC frame was monotonically loaded. This is one of the very few research works that attempted to model a structure that has columns and beams through the use of the 3D detailed modeling approach (hexahedral elements and embedded rebar elements). A numerical study on the FRP strengthening of RC beam-to-column connections under cyclic loading was published by Dalalbashi et al. [35]. In their work, which was based on the work presented by Mahini and Ronagh [36], they used an exterior beam-column joint that was modelled in ANSYS through the use of hexahedral elements (an average of 3,500 elements per model), while the concrete material was simulated through the use of the Hognestad et al. [37] model. The steel rebars assumed a bilinear material model, where the cracking in concrete was accounted for through the smeared crack approach. This is one of the few works found in the international literature that use 3D detailed modeling with cyclic loading conditions to numerically study the response of CFRP retrofitting. Therefore, this highlights the importance of developing an algorithm that will be able to handle full-scale structures using this modeling approach when they undertake this type of loading conditions.

Gribniak et al. [38] used ATENA to numerically validate and study the mechanical behavior of CFRP sheet retrofitted beams (only a quarter of the RC beam was modeled herein), while Duarte et al. [39] used the same software in order to study the effect of repairing RC cracked beams strengthened

with CFRP laminates in 2D. ANSYS software was also used by Nasr et al. [40] so as to study RC beams with openings that were strengthened by using either CFRP or GFRP laminates.

Qapo et al. [41] used DIANA to perform nonlinear monotonic analyses of CFRP-strip retrofitted RC beams. The concrete medium was discretized through the use of hexahedral elements that treat cracking through the smeared crack approach, while the CFRP strips were modelled through the four-node quadrilateral isoparametric curved shell element. The effect of prestress was also accounted for in this work and the numerically obtained curves (push over analyses) were compared to the experimental results. As an overall conclusion, the numerical and experimental curve comparison was characterized by a good agreement between the derived curves but after the nonlinearities increased significantly the numerical curves tended to overestimate the beams' stiffness. ABAQUS was used by Mrozek et al. [42] to investigate the effectiveness of using CFRP composites to strengthen unreinforced masonry walls. Monotonic nonlinear analysis was performed in this work for 2D problems.

More recently, a research work was presented by Mazzucco et al. [43], where ABAQUS was used in order to study the mechanical behavior of confined RC columns retrofitted with CFRP composites under axial loading. Azarm et al. [44] developed an exterior RC joint model that was retrofitted with CFRP composites with ANSYS so as to numerically capture the experimental results that were obtained through monotonic loading conditions. The main finding that derived from this research work was that the overall joint capacity was increasing when the number of CFRP layers was increased, while it was noted that the numerically obtained curves were always stiffer than the corresponding experimental curves (approximately 8-10%). Lampropoulos et al. [45] studied the effect of ultra-high performance fibre reinforced concrete jackets through the use of ATENA under monotonic loading. Finally, Banjara and Ramanjaneyulu [46] used ANSYS to perform 3D nonlinear finite element simulations and study shear deficient and glass fibre reinforced plastic strengthened RC beams under monotonic four-point bending loading conditions.

From the above literature review, it is evident that the scientific community started to recognize the

potentials of using the 3D detailed modeling approach thus the development of robust, accurate and efficient algorithms that can be implemented at a full-scale building level is of significant importance. The numerical instabilities and computational demand when implementing the 3D detail modeling approach are high, limiting the studies to single member structural members under monotonic nonlinear loading analyses. In this research work, the HYMOD approach [1-3], which is integrated in Reconan FEA [47], is used so as to numerically investigate the effect of CFRP jacketing and infill RC shear wall strengthening of a full-scale 4-storey RC building. Four different reinforcement types are also studied herein that foresee the use of Aramid, Glass and Carbon FRP rebars, in addition to the conventional steel reinforcement. These rebar types are used in different FE models as reinforcement within the infill RC shear walls, while the objective is to study the overall and local effect in terms of mechanical behavior when using different rebar materials during the strengthening design. The numerical investigation aims to provide answers to complicated questions that deal with the overall effect of the retrofitting technique in-terms of structural strength and seismic enhancement, and how the framing system of a multistorey realistic RC building will perform under different retrofitting strategies.

Furthermore, one of the main objectives of this research work is to emphasize the importance of developing and using the proper numerical tools when investigating the vulnerability of structures with the intent of developing fragility curves and damage estimations due to seismic loads. Kappos and Dimitrakopoulos [48] and Chrysostomou et al. [49], presented a methodology towards developing decision making guidelines for choosing the optimum strengthening level, based on nonlinear analyses that foresee the use of beam-column finite elements in SAP2000. A more recent work that adopted a similar approach was also proposed by Vitiello et al. [50], where the life-cycle cost optimization of retrofitted RC structures was discussed in an attempt to derive the cost benefit of retrofitting interventions based on the performance of structures under different earthquake acceleration intensities. In their work [50], nonlinear static analyses were performed that did not account for torsional effects nor the occurrence of plastic hinges due to shear deformation. As it was also noted in their work [50], the use of proper tools during the seismic assessment of RC structures is of great

importance thus affects the overall life-cycle cost optimization.

It must be noted at this point that, the development of numerical tools for handling large-scale models for modeling full-scale structures through the use of objective and accurate numerical models [51], is crucial towards establishing any type of conclusions when dealing with the seismic performance of RC structures. It is also evident that the use of the simplistic beam-column finite elements in the development of fragility curves and retrofitting recommendation is not an optimum approach [50] that requires to be reconsidered. For these reasons, this research work has as a main objective to set the base for developing retrofitting recommendations based on objective and accurate numerical tools to support decision-making to select the optimum retrofit strategy of RC structures.

2. Material Modeling

The HYMOD approach for cyclic modeling considers two different types of FE models [52] for discretizing the frame of any building-like structure. These elements are the isoparametric hexahedral element and the beam-column fibre element that is integrated with the natural mode method [1-3]. These FEs have a numerical formulation that is based on three- and one-dimensional domains, respectively, hence two different dimensionalities are combined, where two concrete material models are considered so as to simulate the understudy 4-storey RC building. For the case of the 1D model, the discretization foresees the division of each beam-column section into fibres that have the ability to account for nonlinearities through the bilinear model (see Fig. 1).

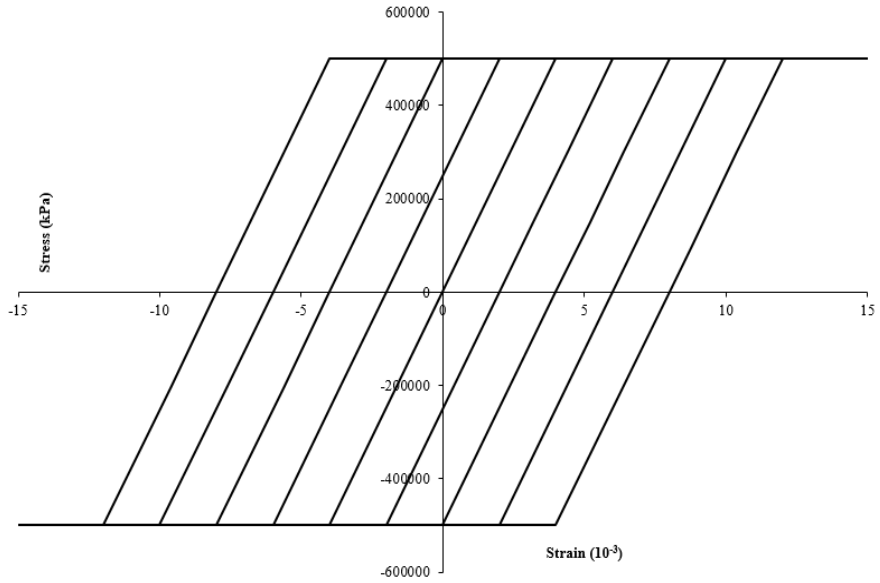

Figure 1. Bilinear model for cyclic analysis [3].

The 3D concrete material model for the cyclic analysis of concrete was presented in [53], which is incorporated into the 8-noded hexahedral elements. The model is based on the Kotsovos and Pavlovic [54] material model, while it was integrated with a flexible crack closure criterion that induces numerical stability during the cyclic analysis as presented in [53]. According to the cyclic concrete material model presented in [55, 56], the smeared crack approach is used to simulate the crack openings in the case of the 3D detailed model. This approach was first presented by Rashid [13] as an extension to the method proposed by Gonzalez-Vidosa et al. [57].

The constitutive matrix of concrete is expressed as follows [53]:

$$\boldsymbol{C}_l^{'} = \begin{bmatrix} a_n\cdot(1-D_c)\cdot(2G_t+\mu) & a_n\cdot(1-D_c)\cdot\mu & a_n\cdot(1-D_c)\cdot\mu & 0 & 0 & 0 \\ a_n\cdot(1-D_c)\cdot\mu & a_n\cdot(1-D_c)\cdot(2G_t+\mu) & a_n\cdot(1-D_c)\cdot\mu & 0 & 0 & 0 \\ a_n\cdot(1-D_c)\cdot\mu & a_n\cdot(1-D_c)\cdot\mu & 2G_t+\mu & 0 & 0 & 0 \\ 0 & 0 & 0 & a_s\cdot(1-D_c)\cdot\beta\cdot G_t & 0 & 0 \\ 0 & 0 & 0 & 0 & a_s\cdot(1-D_c)\cdot\beta\cdot G_t & 0 \\ 0 & 0 & 0 & 0 & 0 & a_s\cdot(1-D_c)\cdot\beta\cdot G_t \end{bmatrix} \quad (1)$$

where β is a retention factor of shear strength at the crack plane and constants a_n and a_s are assumed to have values of 0.25 and 0.125, respectively [53]. The expression in Eq. 1 that describes the anisotropic behaviour of concrete in the local Cartesian coordinate system is transformed into the global system through the use of a basic transformation as given in Eq. 2.

$$\boldsymbol{C}_g = \boldsymbol{T}^T \boldsymbol{C}_l \boldsymbol{T} \tag{2}$$

where $\boldsymbol{T}$ is the corresponding transformation matrix that consists of the direction cosines that define the orientation of the local to global axis; D_c which is expressed through Eq. 3, is a damage factor [53] that describes the accumulated loss of energy based on the current number of times a crack was found to open and close. This is also accounted for in this research work.

$$D_c = e^{-(1-a)/f_{cc}} = e^{-\left(1-\left(1-\frac{\varepsilon_{cr}}{\varepsilon_{\max}}\right)\right)/f_{cc}} = e^{-\left(\frac{\varepsilon_{cr}}{\varepsilon_{\max}}\right)/f_{cc}} \tag{3}$$

Parameter f_{cc} represents how many times a crack has closed and it is updated in every iteration at each Gauss Point within the concrete hexahedral elements. The concrete constitutive matrix is calculated based on Eq. 1 and for the case where a crack is being closed and the stresses have to be corrected through the use of Eq. 4.

$$\boldsymbol{\sigma}^j = \boldsymbol{\sigma}^{j-1} + \boldsymbol{C}_g \cdot \Delta\boldsymbol{\varepsilon}^j \tag{4}$$

In order to introduce a stabilizing factor during the cyclic modelling of extremely cracked concrete regions [55], the modification of the constitutive matrix of a fully crushed Gauss Point takes the following form:

$$\boldsymbol{C}_l' = \begin{bmatrix} \beta_c\cdot(1-D_c)\cdot(2G_t+\mu) & 0 & 0 & 0 & 0 & 0 \\ 0 & \beta_c\cdot(1-D_c)\cdot(2G_t+\mu) & 0 & 0 & 0 & 0 \\ 0 & 0 & \beta_c\cdot(1-D_c)\cdot(2G_t+\mu) & 0 & 0 & 0 \\ 0 & 0 & 0 & \beta_c\cdot(1-D_c)\cdot\beta\cdot G_t & 0 & 0 \\ 0 & 0 & 0 & 0 & \beta_c\cdot(1-D_c)\cdot\beta\cdot G_t & 0 \\ 0 & 0 & 0 & 0 & 0 & \beta_c\cdot(1-D_c)\cdot\beta\cdot G_t \end{bmatrix} \tag{5}$$

where $\beta_c = 0.025$ which is a parameter similar to β that represents the shear strength retention factor. For more information on the 3D concrete material model see [55].

For the case of the steel embedded rebar elements found within the hexahedral mesh, they are modelled through the use of the Menegotto-Pinto [58] model that takes into account the Bauschinger effect. Based on [53], a damage factor was proposed to account for the accumulated damage of the concrete domain around the embedded rebar. Therefore, the parameters *a,* as expressed in the Eq. 7,

can be used to determine the damage level D_s of concrete by using Eq. 6.

$$D_s = \left[1 - a_{Element}\right] \tag{6}$$

$$a_{Element} = \frac{\sum_{1}^{n_{cr}} a_i}{n_{cr}}, \tag{7}$$

where n_{cr} represents the number of current cracked Gauss Points in a given hexahedral element. According to the adopted formulation [53], during unloading and at the point where the structure reaches its initial deformation, the material deterioration of the rebars can be calculated as:

$$E_s^{'} = (1 - D_s) E_s \tag{8}$$

In addition to the proposed modification in [53] and in order to capture pinching effects at the material level, the implementation of a reduced parameter R of the steel model was proposed in [55]:

$$R = R_0 - \frac{a_1 \xi}{\alpha_2 + \xi} \tag{9}$$

Parameters R_0, a_1 and a_2 were determined through the performance of extensive numerical tests presented in [53] and are assumed to be equal to 20, 18.5 and 0.15, respectively. By using the same concept described above and as presented in [53], the reduction factor D_R was proposed in [55] in order to decrease the parameter R into R' which is calculated as:

$$R^{'} = (1 - D_R) R \text{ , where } D_R = D_s \tag{10}$$

This was found to provide the model with the ability to capture pitching effects during extreme cyclic loading conditions that lead to excessive cracking and slippage.

In this research work, the CFRP jacketing was also discretized in detail by using the 8-noded hexahedral element, where the material model used in simulating the stress-strain relationship for the CFRP jacketing, foresaw a linear behavior until complete failure for both tension and compression states, as illustrated in Fig. 2. Tensile and compressive strengths were assumed to be equal at the material level for all analyses performed in this research work.

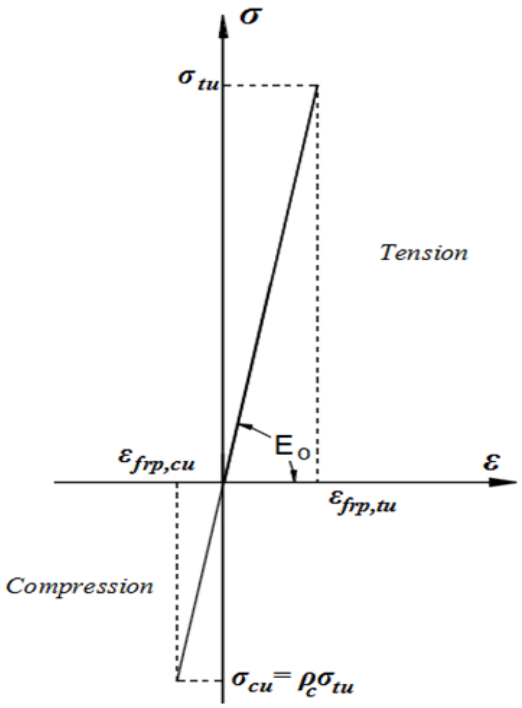

Figure 2. Material model of CFRP jacketing. [59]

As it was discussed in [35], in order to avoid any intermediate crack-induced debonding failure mode during the FE analysis, the maximum strains of the FRP sheets should be checked ensuring that they will not exceed the limiting values suggested by ACI 440.2-08 (2008). Based on the ACI recommendations, debonding might occur for a strain level of ε_{fd} that is computed based on Eq. 11.

$$\varepsilon_{fd} = 0.41\sqrt{\frac{f_c'}{nE_f t_f}} \leq 0.9\varepsilon_{fu} \tag{11}$$

where, f_c' is the compressive strength of concrete, E_f is the elastic modulus of the FRP material, t_f is thickness of the FRP fibres, n is the number of FRP layers and ε_{fu} is the ultimate tensile strain of the FRP. Given that the structural members that will be examined in the following sections foresee a proper anchorage between the CFRP sheet and concrete, the FE models will assume a full bonding. This numerical assumption, even though it is adopted by researchers [29, 35, 36], it is expected in some cases to affect the numerical response of the models near the failure load deriving a stiffer numerical response.

3. Validation Models

3.1 Monotonic Loading

As it was mentioned above, all the analyses were performed through the use of Reconan FEA [47] research software that is integrated with the ability to analyse RC structures through the use of nonlinear cyclic analysis. The HYMOD was experimentally tested and found to be able to capture the cyclic mechanical behavior of RC joints [1-3], whereas the use of CFRP sheets was not studied in the parametric investigation presented in [2]. For this reason, and so as to further validate the ability of the developed algorithm to capture the mechanical behavior of RC joints with CFRP jackets [55], the Mahini and Ronagh [36] experiments are going to be tested herein. Two different specimens were studied in this section under monotonic loading, the RSC1 and RSM2 joints that foresaw the use of 3 layers of CFRP sheets and a sheet length $l_f = 200\ mm$ (see Fig. 3). Based on their report, the thickness of the CFRP sheets for these two specimens was 0.495 mm and the uniaxial compressive strength of concrete was 36.44 and 40.75 MPa for the RSC1 and RSM2 specimens, respectively.

Two HYMOD meshes were developed so as to simulate the two specimens as shown in Fig. 4. The two models foresaw the modeling of the column with 8-noded hexahedral elements, where the beam was partially discretized through the use of the beam-column FE and the rest through the use of the 8-noded hexahedral with embedded rod elements. The plastic hinge which includes the CFRP sheet had a length of 42.5 cm and corresponds to a $1.84h$, where h is the beam's section height. The total number used to discretize the joint was 120 hexahedral elements, 224 rod elements (embedded rebars) and 1 beam-column FE. A 30 kN concentrated force was applied at the beam's tip incrementally through the use of 50 Newton-Raphson load steps. The energy convergence tolerance was set to 10^{-5} for both analyses. According to the experimental findings presented in [35], the RSC1 specimen developed a 21.32 kN maximum load, while the RSM2 specimen a 21.12 kN.

Fig. 5 shows the comparison between the experimental and numerically obtained curves. It can be seen that the HYMOD simulations managed to capture the experimental curves and the overall mechanical behavior of the two specimens. It is also easy to observe that the numerical models manage

to accurately capture the stiffness of the two specimens while the numerical behavior becomes stiffer as the load increases. This is attributed to the full bond assumption that does not allow the model to account for the slippage that might occur at high load levels. Nevertheless, the developed models manage to capture the maximum failure load in an accurate manner (see Fig. 5). For the case of the RSC1 specimen, the experimental curve represents the envelope curve up to the point of the maximum load during the cyclic test. It must be noted at this point that, the total number of FEs that were used to discretize the joints was 345 that makes it 10 times less than the corresponding number of FEs used in [35], thus the required computational time in order to solve the nonlinear problem herein was less than a second. The analyses were performed through the use of a 4.2 GHz core.

It must be noted here that, additional verification analyses on the developed algorithm [1-3] were performed and presented in [55], where the study of severely damaged RC joints was discussed for both bear and CFRP retrofitted specimens that were tested under ultimate limit state cyclic loading conditions.

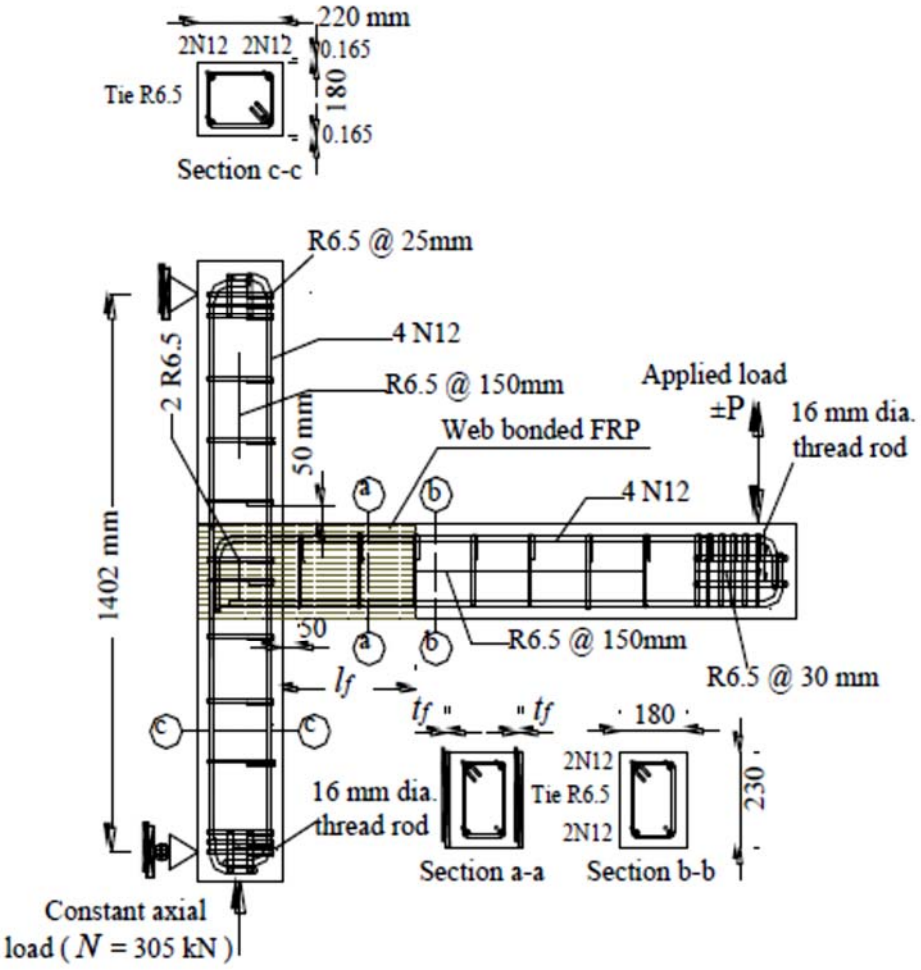

Figure 3. Geometry and reinforcement details of the beam-column joints tested by Mahini and Ronagh (as found in [36]).

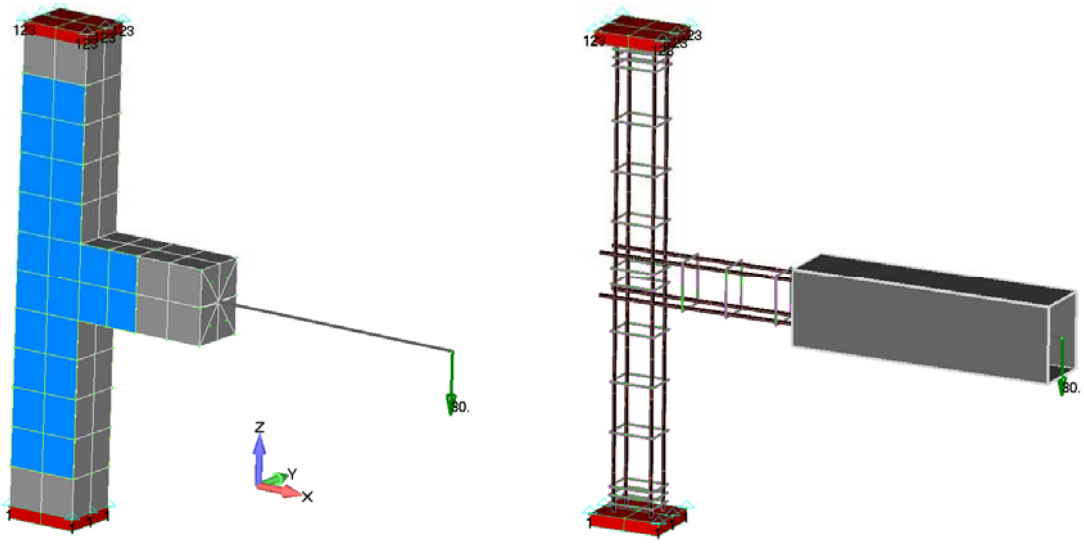

a. **b.**

Figure 4. FE HYMOD mesh of RSC1 and RSM2 specimens. (a) Hexa elements and (b) Embedded rebar elements.

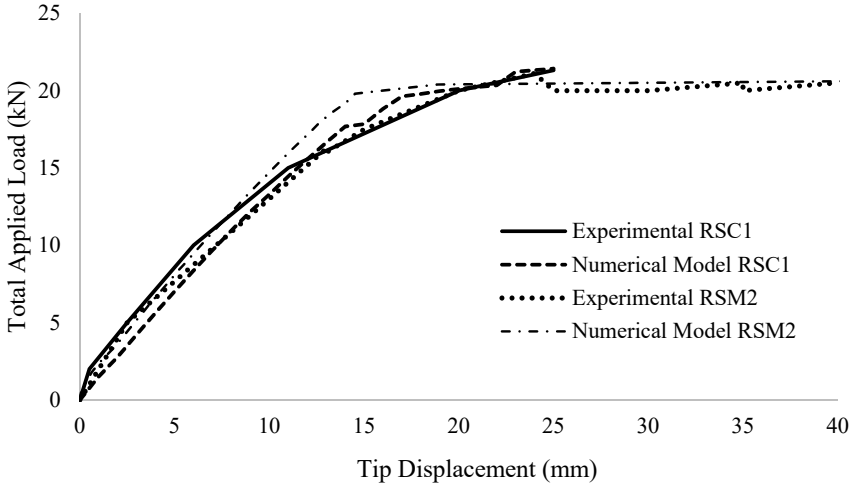

Figure 5. Comparison between the experimental and numerical curves for the beam-column joints tested by Mahini and Ronagh [36].

3.2 Cyclic Loading

As it was stated above, the developed algorithm was validated in [55] when it comes to its ability to capture extreme pinching of RC bare and CFRP jacketing retrofitted structures. To further validate the ability of the developed algorithm to predict the mechanical response of CFRP retrofitted RC structures, specimen JC2RF tested in [66] is modelled and analysed herein. Fig. 6 shows the general geometry of the specimen and the reinforcement details according to the test performed in [66]. The main objective of this work [66], was to design RC joints that foresaw for insufficient confinement and anchorage length within the RC joint, where ultimate limit state cyclic loading was applied complete failure. The tested bare joints were then rehabilitated and strengthened with CFRP jackets, where the ultimate cyclic loading was performed again in an attempt to investigate the retrofitting effectiveness.

Table 1 shows the concrete material properties as they derived from standard testing on cylinders, where the yielding stress of the rebars used to reinforce the specimen were 551 and 612 MPa for the Ø16 and Ø8 rebars, respectively. The tensile strength of the CFRP material was reported to be equal to 4,140 MPa with an ultimate failure strain of 1.7% [66]. These were also the values defined within the numerical model presented in Fig. 7, which shows the hexahedral and embedded finite element meshes that were developed to discretize specimen JC2RF. The beam was loaded in displacement

control using a servo-hydraulic actuator [66]. Three push-pull cycles were applied at drift ratios δ (δ=beam tip displacement/beam length) of ±0.25%, ±0.5%, ±1.0%, ±2.0%, ±3.0%, ±4.0% and ±5.0%. The nonlinear cyclic analysis foresaw a total of 410 displacement increments and an energy convergence tolerance of 10^{-5}.

Table 1 Material characteristics of beam-column joints JC2 and JC2RF [66].

ID	f_{cm} (MPa)	f_{ctm} (MPa)	Test conditions
JC2	32.0	2.44	Original bare joint, detailing C
JC2RF	56.9	3.61	JC2 retested with new recast core and CFRP retrofit

*Note: All values refer to the unconfined strength of concrete in compression and tension.

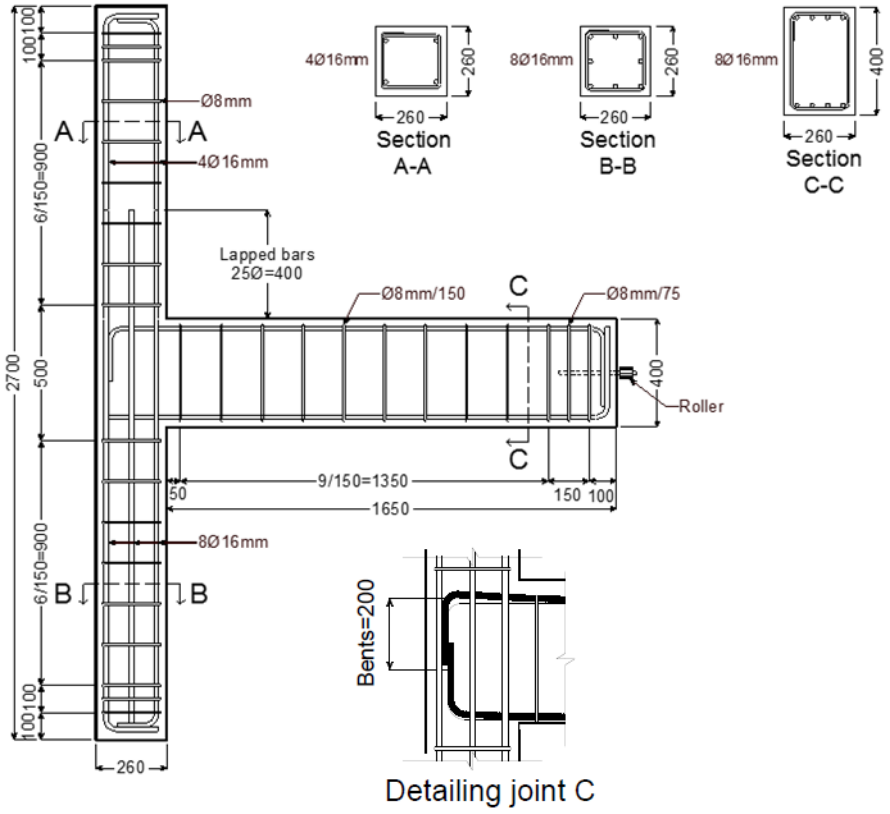

Figure 6. Geometry and reinforcement details of RC joint (units: mm) [66].

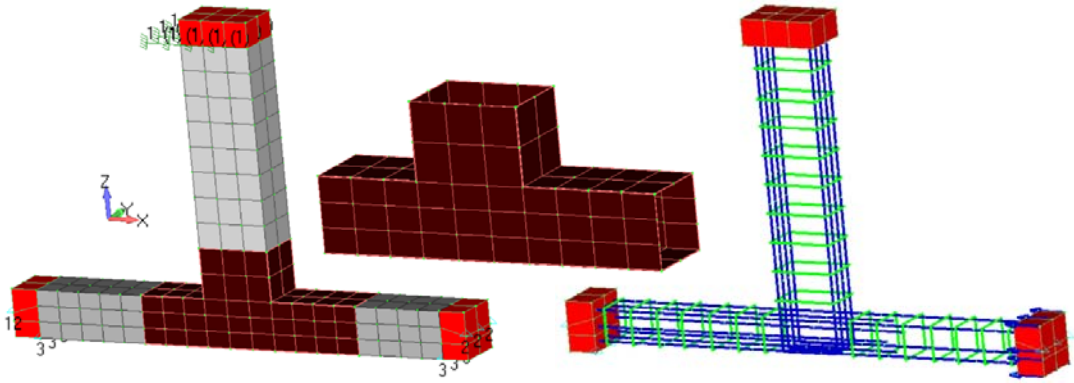

Figure 7. Finite element mesh of the (Left) full model, (Centre) CFRP jacketing and (Right) embedded rebar elements.

Fig. 8 shows the comparison between the experimental and numerical curves of specimen JC2RF as it resulted from the numerical investigation performed for the needs of this research work. It is easy to observe that the numerically obtained curve is in a good agreement with the experimental data, where the maximum positive numerically computed load was found to be equal to 119.43 kN, whereas the experimental maximum [66] was reported to be equal to 120 kN. The corresponding maximum negative load that was numerically obtained was equal to 115.7 kN, where the equivalent experimental value as seen in Fig. 8 is equal to 114 kN. Furthermore, the ability of the proposed algorithm to capture the effectiveness of the retrofitting in terms of strength enhancement is evident, where the extreme pitching caused by slippage and excessive cracking phenomena is also easy to observe.

Additionally, the strength deterioration as the loading cycles increase is easily depicted in Fig. 8, demonstrating the ability of the newly proposed material damage factors to capture the material deterioration of concrete as the number of cycles increases. It is also interesting to note at this point that the numerical model failed during the final cycle, where a total of 5% drift ratio was applied. Out of the two final cycles that foresaw a 5% drift ratio, the numerical analysis managed to solve 1.5, where the numerical analysis stopped due to excessive unbalanced forces derived from the damage developed at the joint. According to the numerical findings of this section, the parametric investigation was performed by adopting the proposed modelling approach [55] to evaluate the cost of two different types of strengthening as it is going to be presented below.

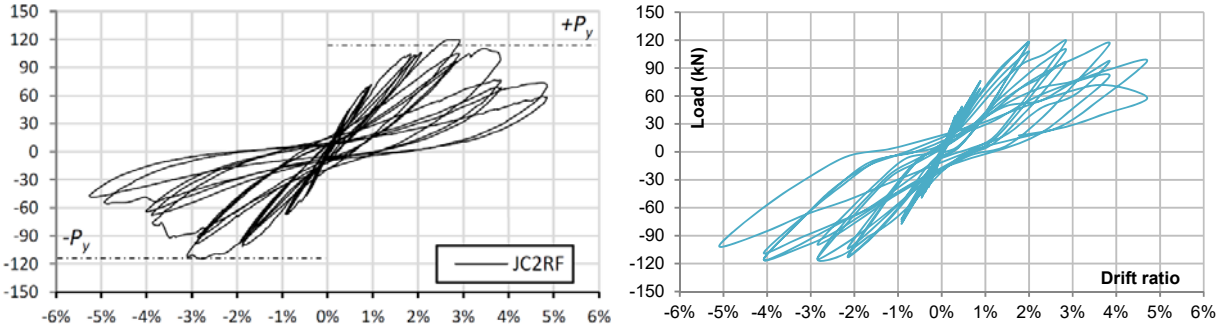

Figure 8. (Left) Experimentally [66] and (Right) numerically obtained load vs drift ratio curves.

4. Finite Element Meshes and Loading Campaign

The parametric investigation that was performed and presented in this section, foresaw the study of two different retrofitting techniques applied on a 4-storey RC building [3]:

a. CFRP sheet jacketing

b. Infill RC shear walls

In addition, the Infill RC shear walls were reinforced with four different types of rebar materials:

i. Steel

ii. Glass fibre reinforced polymer (GFRP)

iii. Aramid fibre reinforced polymer (AFRP)

iv. Carbon fibre reinforced polymer (CFRP)

Based on the numerical investigation performed in [3], the 4-storey retrofitted RC specimen that was studied in [60], undergone three cyclic loading histories that were scaled to represent different seismic acceleration levels. The last loading history that was applied (funeral load cycles), foresaw the loading of the structure up to its maximum carrying capacity. Based on the experimental data found in [60], the funeral cycles managed to apply a 2,025 kN along the positive x-axis and a 2,032 kN along the negative direction, horizontally displacing the structure 89 and -125 mm, respectively.

As it was presented in [3], one of the numerically challenging factors when modeling this experimental setup is accounting for the material damage that occurred in the 1st and 2nd sets of cyclic

loading prior to applying the 3rd and final load history that would push the structure to its maximum capacity limits. In order to establish a realistic loading configuration, Markou et al. [3] proposed the loading history shown in Fig. 9, which foresees the application of seven preparatory loading cycles so as to induce the damage which occurs due to the first two tests, thus continuing with the application of the final set of displacements based on the experimental data.

The 24 models that were developed here for the needs of the numerical experiment presented in this work, were all based on the models discussed in [3], whereas the details in regards to each finite element model can be seen in Table 1. The models assume the use of different intervention approaches, where the first 9 models (BC203-BC513) foresee the study of the CFRP sheet jacketing (3 layers) applied on the initial bare frame BC00. Fig. 10 shows the finite element mesh of model BC503 that foresees the strengthening of the base and head of all columns of the structure, while Fig. 11 shows the corresponding mesh for the case of model BC413 that foresees the strengthening of all beams and columns of the structure except from the last floor. It must be noted here that the BC00 model that was developed to study the mechanical behavior of the initial frame without any strengthening interventions, uses the same model as the one represented in Figs. 10-11, where the hexahedral elements used to discretize the CFRP sheets are deleted.

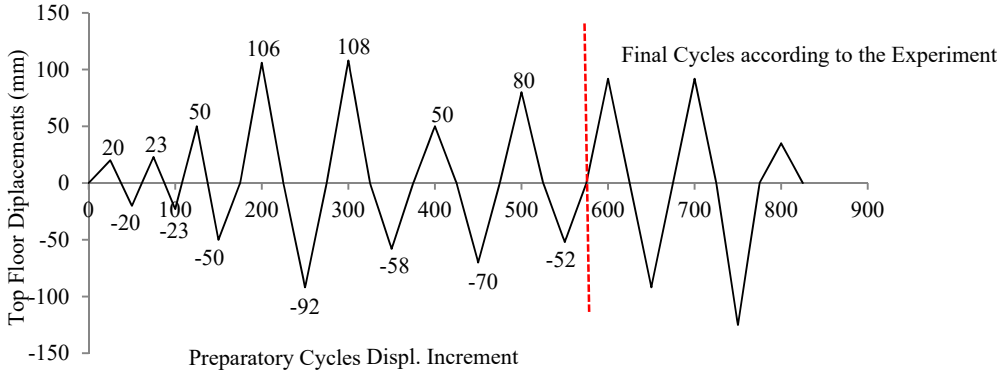

Figure 9. Displacement history applied at the top floor of the specimen.

Table 2. HYMOD meshes for the parametric investigation of different interventions.

a/a	Model Code	Infill Wall	Type of rebars inside the Infill RC shear walls	CFRP Sheet Jacketing	Number of CFRP layers
1	BC00	-	-	-	-
2	BC203	-	-	Ground floor columns - base and head	3
3	BC303	-	-	Ground and 1st floor columns - base and head	3
4	BC403	-	-	Ground, 1st and 2nd floor columns - base and head	3
5	BC503	-	-	All floor columns - base and head	3
6	BC213	-	-	Ground floor columns and beams	3
7	BC313	-	-	Ground and 1st floor columns and beams	3
8	BC413	-	-	Ground, 1st and 2nd floor columns and beams	3
9	BC513	-	-	All columns and beams	3
10	BC205	-	-	Ground floor columns - base and head	5
11	BC305	-	-	Ground and 1st floor columns - base and head	5
12	BC405	-	-	Ground, 1st and 2nd floor columns - base and head	5
13	BC505	-	-	All floor columns - base and head	5
14	BC215	-	-	Ground floor columns and beams	5
15	BC315	-	-	Ground and 1st floor columns and beams	5
16	BC415	-	-	Ground, 1st and 2nd floor columns and beams	5
17	BC515	-	-	All columns and beams	5
18	RC00	Yes	Steel	-	-
19	RC10	Yes	Steel	Ground floor wall edges	5
20	RG10	Yes	GFRP	Ground floor wall edges	5
21	RA10	Yes	AFRP	Ground floor wall edges	5
22	RCC10	Yes	CFRP	Ground floor wall edges	5
23	BC1F	Yes	Steel	Infill shear wall placed at the ground floor with only CFRP sheets at the edges	5

24	BC2F	Yes	Steel	Infill shear wall placed at the ground and 1st floor only with CFRP sheets at the edges of the ground floor walls	5

Table 3. FRP and steel rebar material properties within the Infill RC shear walls.

a/a	**Rebar Material**	**Young Modulus (GPa)**	**Ultimate Stress (MPa)**
1	Glass FRP	50	650
2	Aramid FRP	80	1,200
3	Carbon FRP	300	2,400
4	Steel	190	400

Additionally, the next 8 models (BC205-BC515) study the case of the initial bear framing system that uses 5 layers of CFRP sheet jacketing placed at different locations within the frame (columns and beams as described in Table 2). Model RC00 foresees the study of the frame that is strengthened by using infill RC shear walls throughout the height of the structure, without any CFRP sheets. The next 5 models assume the use of the infill wall as the main retrofitting system, where different rebar materials are investigated (four reinforcement materials inside the Infill RC shear walls are assumed; see Table 3 for FRP rebar material properties). The model that was developed for the needs of this group of structures can be seen in Fig. 12. Finally, as can be depicted from Table 2, model BC1F foresees the placement of infill RC shear walls on the ground floor, while model BC2F assumes infill RC shear walls at the ground and 1st floor only (see Fig. 13). These two models were developed and studied in [3], whereas the derived results are also used herein for the needs of this investigation.

It must be noted at this point that the building had two 4-storey parallel frames connected through a continuous slab of 15 cm thickness and four out-of-plane central beams that connected the two frames between them (Fig. 10). Each frame consisted of 3 bays with an 8.9 m total span, with the central bay infilled with a RC wall 2.9x0.25m (2.1 m net span and 0.25 m thickness; see Fig. 12). The structure had a total height of 12 m and the distance between the South and North frames was 6.25 m.

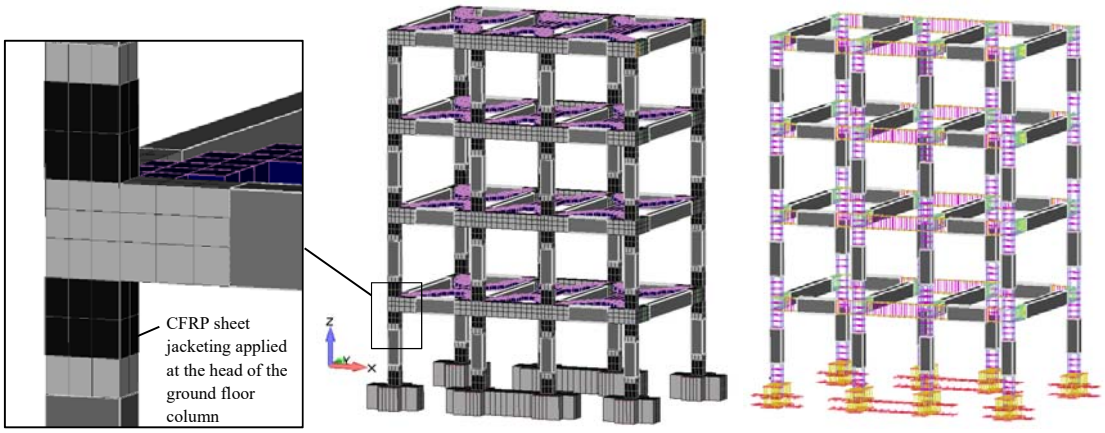

a. b.

Figure 10. FE mesh of model BC503. Bear frame with CFRP sheet jacketing. (a) Concrete and (b) reinforcement mesh.

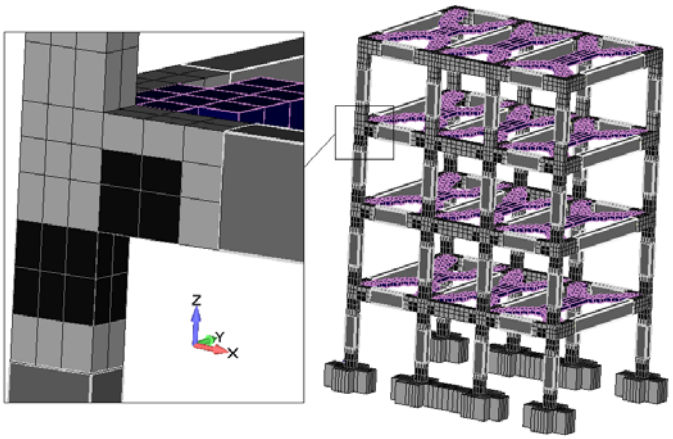

Figure 11. FE mesh of model BC413. RC and CFRP hexahedral finite elements.

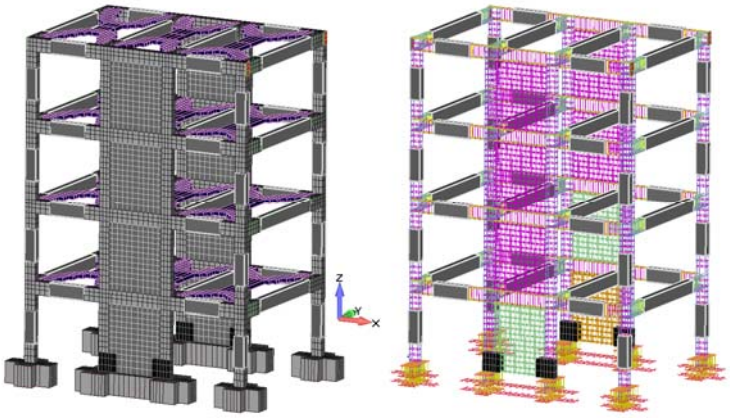

a. b.

Figure 12. FE mesh of model RC10. Frame with infill walls and CFRP sheet jacketing at the edges of the ground floor walls. (a) Concrete and (b) reinforcement mesh.

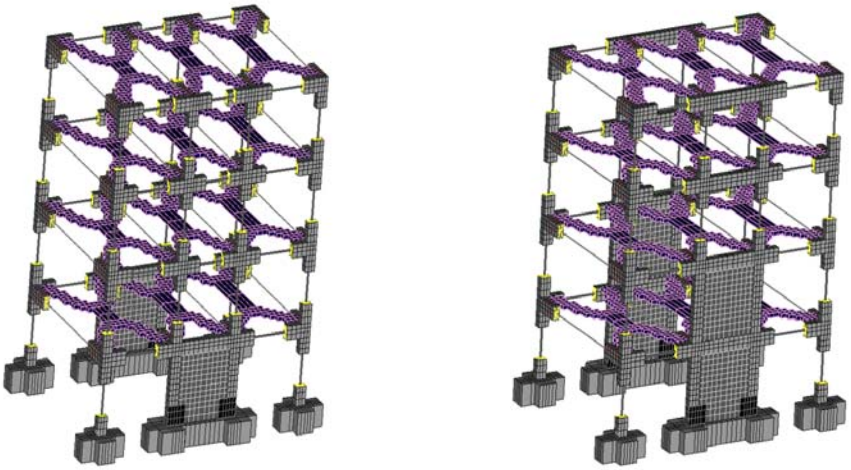

a. b.

. 3 **Figure. 13**D mesh view of the 4-storey RC building with infill RC walls at the (a) ground floor and (b) ground and first floors. [3]

5. Numerical Results and Discussion

The analyses that were performed of the needs of this research work adopted an energy convergence criterion as expressed in the Eq. 12. A convergence energy tolerance of 10^{-5} was used to reassure numerical stability and maximum accuracy during the nonlinear cyclic analyses. It must be noted at this point that the CPU used to perform all the analyses presented in this work had a core of 3.7 GHz and 64 Gb RAM.

$$e_{er} = \frac{\Delta u_s^j \| F_s^{t+\Delta t} - R_s^{t+\Delta t} \|}{\Delta u_s^1 \| F_s^{t+\Delta t} - R_s^t \|} \leq tolerance \tag{12}$$

5.1 Hysteretic Behavior and Strength Enhancement

In order to derive comparable results, thus extract objective conclusions in regards to the overall mechanical hysteretic response of each retrofitting intervention, all models were analysed by using the same displacement history shown in Fig. 9. This approach led to cases where some structures did not manage to finish with the entire displacement history due to premature failure, whereas structures that were reinforced with CFRP throughout the hull building height exhibited an increased hysteretic behaviour and strength. For this reason, the displacement history diagram was modified accordingly for each retrofitting case to ensure that the complete imposed displacement history was solved for all

the models.

As can be seen in Fig. 14, some models failed in the final cycles before reaching the last imposed displacement, therefore, the maximum imposed displacements were decreased accordingly. Models BC415 and BC515 managed to undertake the imposed displacements according to Fig. 9, whereas BC215 and BC315 required a modification of the imposed displacements (from a maximum horizontal negative 125 mm to 110 mm). Similarly, Figs. 15 and 16, show cases where the imposed displacements decreased for both the preparatory and final cycles of the diagram. Finally, the models that were strengthened throughout their height exhibited an increased capacity and hysteretic behaviour, thus their final cycles according to the numerical experiment [3] were increased to investigate their ability to deform beyond the 92 mm of horizontal deformation (Figs 14-17).

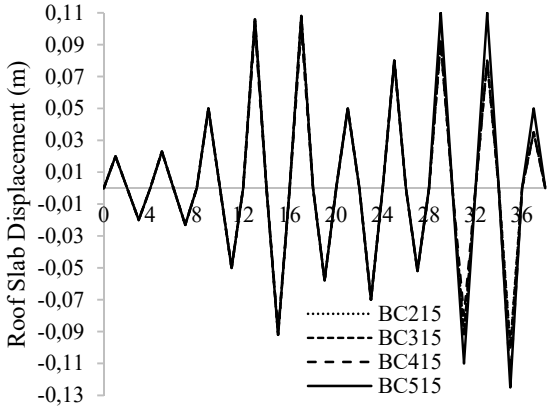

Figure. 14. Displacement history applied at the top floor of the specimens BC215-BC515.

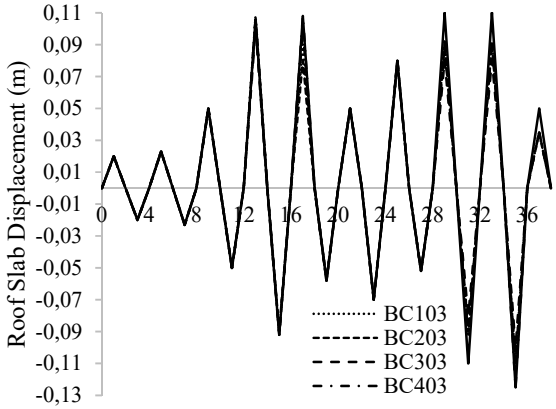

Figure. 15. Displacement history applied at the top floor of the specimens BC203-BC503.

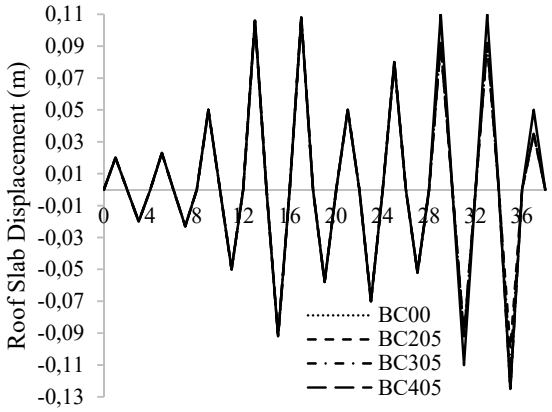

Figure. 16. Displacement history applied at the top floor of the specimens BC205-BC505.

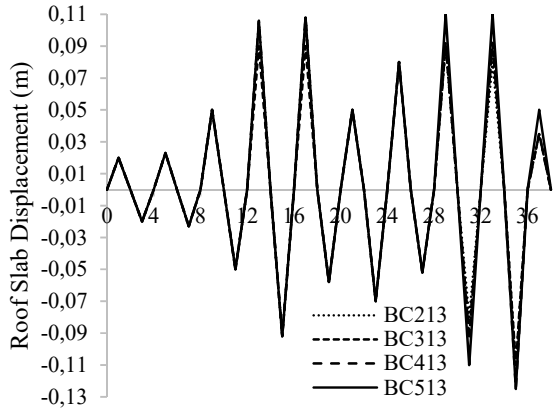

Figure. 17. Displacement history applied at the top floor of the specimens BC213-BC513.

Before presenting and discussing the numerical findings on the hysteretic behaviour of the 24 models, the comparison between the modeling approach that assumes material damage factors [3] and the recently published approach that recommends the use of material damage factors for concrete and steel [55, 56], is performed. To highlight the importance of the newly proposed material damage factors, model BC205 was used, where it was solved for both cases (with and without damage factors). As it was discussed in [55], the damage factors account for the accumulated damage in concrete affecting both steel rebars and concrete domains based on the number of openings and closings of a crack at a specific integration point. Therefore, the damage factors [55, 56] are directly connected to the number of opening and closing of cracks at the Gauss point level of a hexahedral element, where the ability of objectively capturing the accumulated damage in both concrete and steel materials is now feasible. Material damage factors [55] were assumed to be active throughout the nonlinear cyclic analyses presented in this research work (see Eqs 3, 6 and 10).

Fig. 18 shows the comparison between the two models that were developed to simulate the hysteretic behaviour of BC205. The two FE models that were analysed herein foresaw the exact same discretization and material properties, where the only difference was the use or not of the material damage factors. It is easy to observe (Fig. 18) that the dashed curve (damage factors active) exhibited a decreased strength for both the positive and negative maximum horizontal displacements, whereas the dissipated energy that derived from the two models was significantly affected by the use of the damage factors. The significant hysteretic dissipated energy difference between the two numerical models is attributed to the joints of the frame where the opening and closing of cracks was found to be significant, while the slippage and concrete damage was present. Therefore, by activating the damage factors [55] the simulation was able to produce a more objective prediction of the mechanical behaviour of the frame that undertook this ultimate cyclic displacement history, leading to significant accumulated damage resulting into both the decrease in terms of overall strength and dissipated energy.

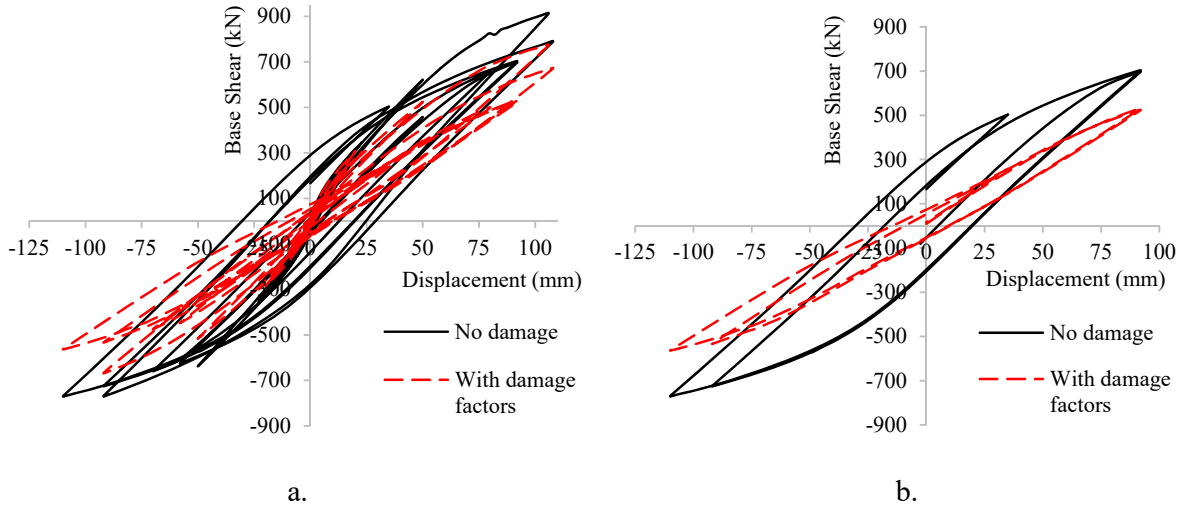

Figure. 18. HYMOD Models BC205. Hysteretic behaviour of the model with and without material damage factors.

(a) Full and (b) final loading cycles.

(b)

Fig. 19 shows the hysteretic behavior of the RC frame without retrofitting and the buildings that were retrofitted with three layers of CFRP sheet only at the columns (BC203-BC503). The first numerical finding from this investigation is the increase of the remaining resistance of all the frames when they are retrofitted with three layers of CFRP sheets. As it was expected, the BC503 model that foresaw the retrofitting of all columns found at the four storeys derived the highest resistance equal to 813 kN during the maximum horizontal deformation of the final cycles, an overall capacity increase of 42.3%. According to Fig. 19, the initial bare RC frame BC00 derived a corresponding 571.3 kN maximum base shear during the final loading cycles (for δ_x = -110 mm). This indicates the overall effect of the retrofitting of columns under cyclic loading conditions, where it is evident that a uniform application of the CFRP sheets throughout the height of the building results into a higher final capacity.

An additional observation can be made for the results obtained by the BC513 model's mechanical behavior that foresaw the retrofitting of all columns and beams with three layers of CFRP sheet. Fig. 20 (BC213-BC513) shows that the remaining strength of this retrofitting configuration managed to derive a maximum capacity of 881 kN, which represents a 54.2% increase in-terms of total base shear during the final cycles of the displacement history. In addition to that, Figs. 19 and 20 indicate an increase in-terms of stiffness, where the retrofitted models are found to exhibit higher remaining

stiffness compared to the initial RC frame (BC00) during the last stages of the cyclic loading history.

Similar conclusions can be drawn from Figs. 21 and 22, where the hysteretic behavior of the models that were retrofitted with five layers of CFRP sheets can be seen. It is evident that the models that assume retrofitting throughout the height of the building derive the highest capacity during the final stages of the cyclic loading (BC505 and BC515), whereas the retrofitting strategy that assumes retrofitting of both columns and beams exhibits the highest remaining resistance. Based on the numerical results, model BC505 derived a 1100 kN maximum base shear, while the BC515 model resulted in a 1,142 kN maximum capacity. These values represent a 92.5% and 99.9% strength increase when strengthening the initial RC frame according to the retrofitting strategies implemented in models BC505 (five CFRP layers at columns only) and BC515 (five CFRP layers at columns and beams), respectively.

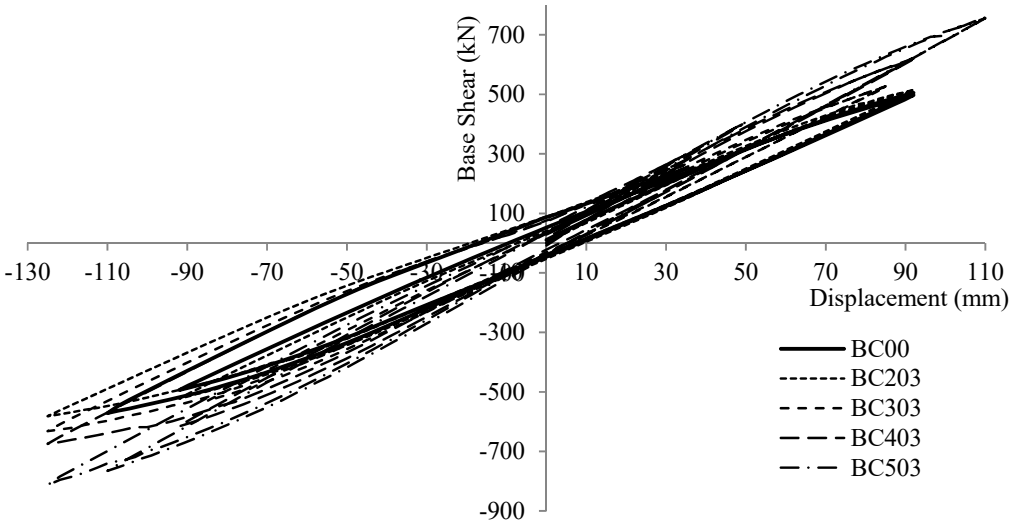

Figure. 19. HYMOD Models BC00 and BC203- BC503. Final cycles. Total base shear-horizontal displacement of the top floor.

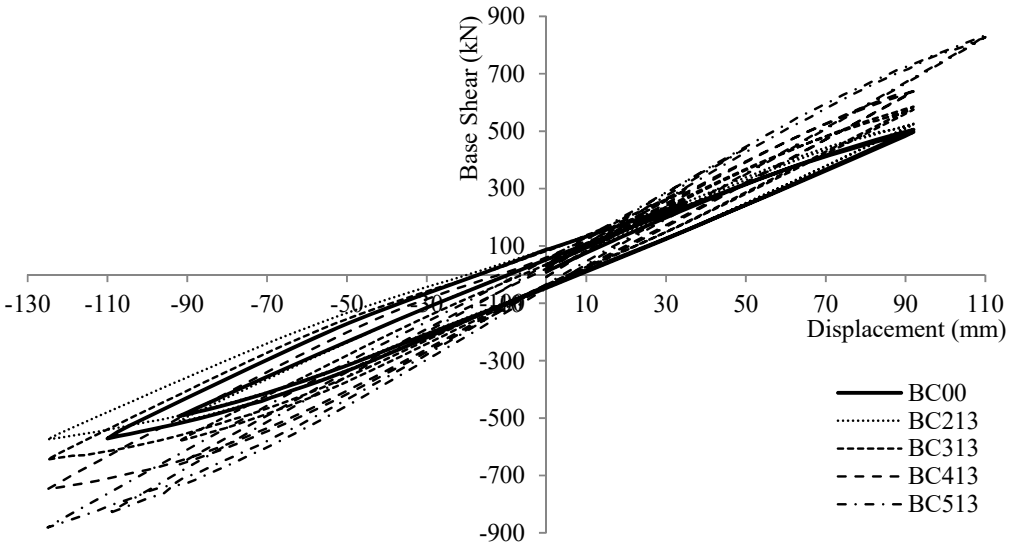

Figure. 20. HYMOD Models BC00 and BC213- BC513. Final cycles. Total base shear-horizontal displacement of the top floor.

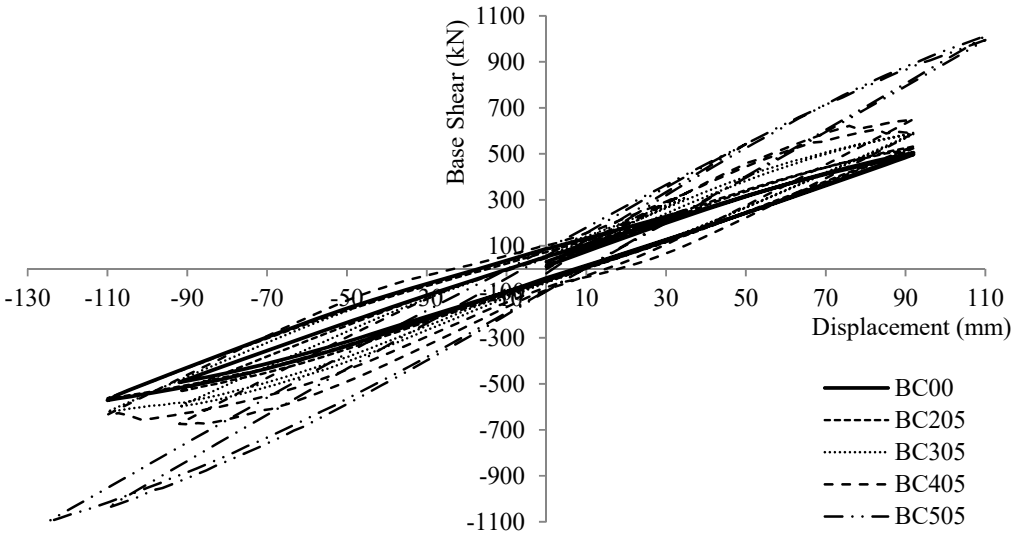

Figure. 21. HYMOD Models BC00 and BC205- BC505. Final cycles. Total base shear-horizontal displacement of the top floor.

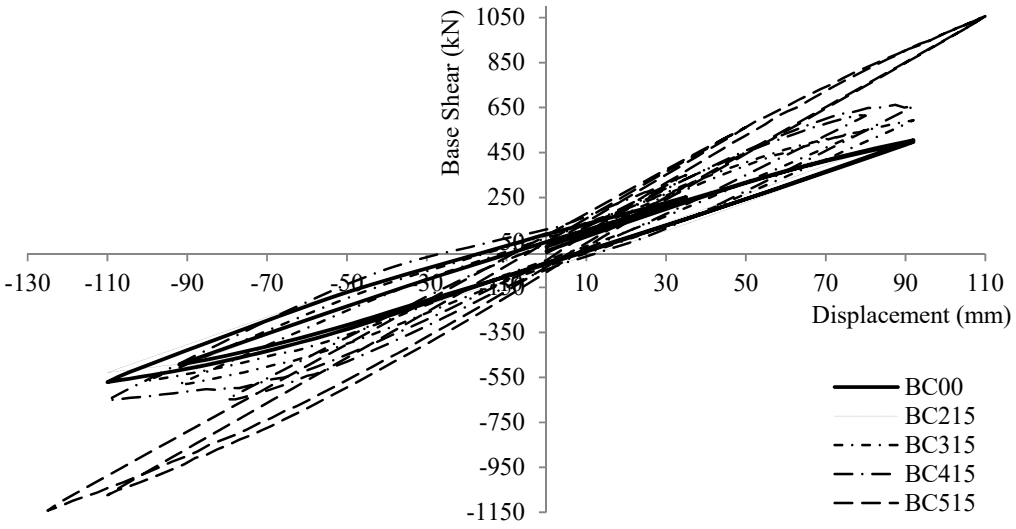

Figure. 22. HYMOD Models BC00 and BC215- BC515. Final cycles. Total base shear-horizontal displacement of the top floor.

The maximum base shear exhibited during the final cycles of the loading history by the frames without infill RC shear walls can be seen in Fig. 23, where it is easy to observe that the last model derived the highest base shear resistance and model BC00 (initial RC frame) the minimum out of all the retrofitted models. One interesting finding was the increased strength of models BC213-BC513 (three CFRP layers at columns and beams) in comparison to the models that assumed five CFRP layers at the columns only (BC205-BC505). The models that were retrofitted with three CFRP layers at both columns and beams derived a higher strength in comparison to the five layers retrofitting of the columns only. The only exception was the BC505 model that derived an increased performance in comparison to the BC513 model. This indicates that using more CFRP in a concentrated manner is not as effective as using the retrofitting material in an optimum way throughout the structure.

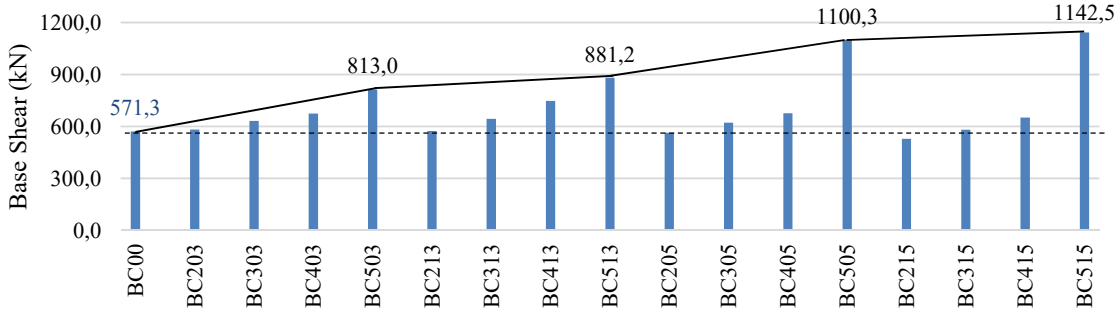

Figure. 23. Maximum base shear derived during the final loading cycles. Retrofitted structures with CFRP sheets without infill RC shear walls.

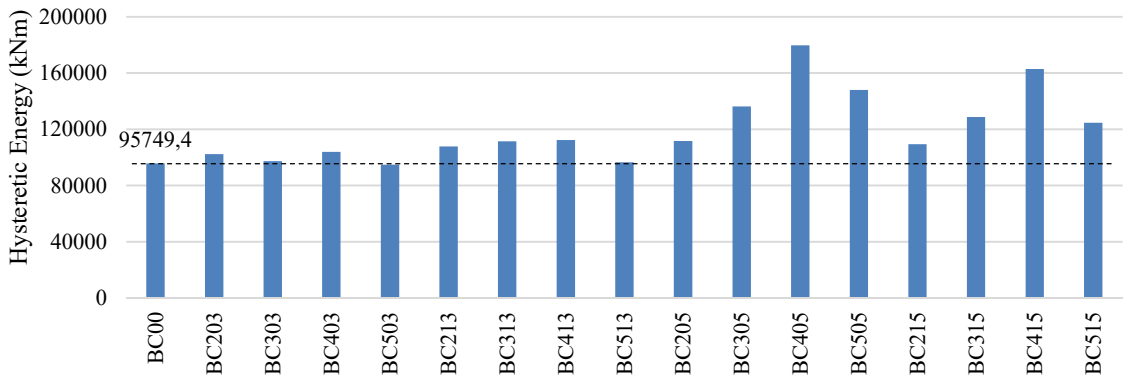

Figure. 24. Hysteretic Energy derived from the full loading history. Retrofitted structures with CFRP sheets without infill RC shear walls.

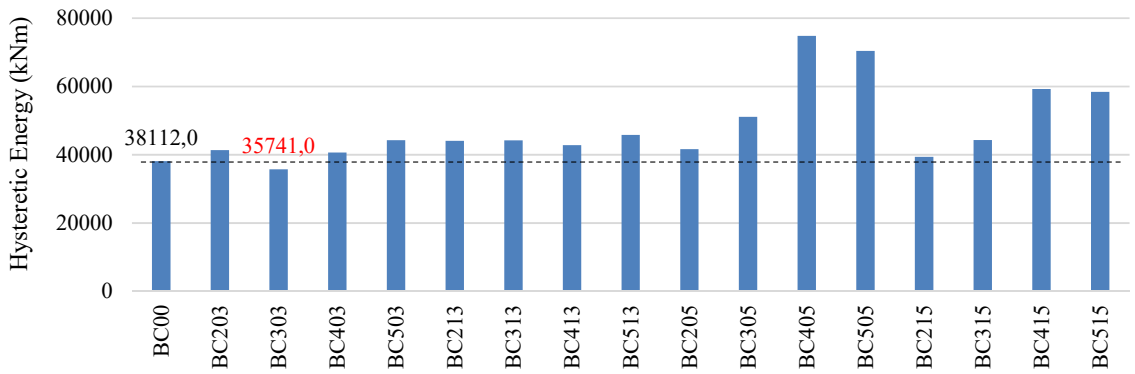

Figure. 25. Hysteretic Energy derived from the preparatory loading cycles. Retrofitted structures with CFRP sheets.

Fig. 24 shows the energy dissipation of each model retrofitted with CFRP sheets without infill RC shear walls for the full displacement history analysis, where it is evident that the models that foresaw retrofitting, derived higher energy dissipation than the bare frame. Additionally, the model BC405 was found to develop the largest hysteretic loops out of all the under-study models that did not foresee the use of infill RC shear walls. This finding is attributed to the development of damage at the non-retrofitted structural members at the joints of the frame that led to rebar yielding, thus larger hysteretic loops. This phenomenon was also reported in [3] where the non-retrofitted beams at joints that were connected to columns that were strengthened, developed concentrated damage thus resulting in higher nonlinearities.

As it can be seen in Fig. 25, model BC303 was found to develop 6% lower energy dissipation compared to the initial RC frame during the preparatory loading cycles, even though its strength in-terms of base shear resistance demonstrated an increase of 10.7% as it is shown in Fig. 23. This

numerical finding illustrates the complexity of estimating the overall mechanical behaviour of CFRP retrofitted RC buildings given that their mechanical response is not only controlled by the behavior of the "retrofitted sections" under monotonic loading conditions, but also by the retrofitting strategy, the overall response of the joints and the local damage that develop at the material level based on the stiffness distribution of each member connected to each joint. An additional significant simplification assumption that is performed when using the simplistic beam-column FE is the deletion of the actual joints, which is modelled with a single node. When discretizing the frame with the HYMOD approach, each joint is modelled as a 3D structural member that captures the mechanical behaviour of this shear dominated structural member in an accurate and exact manner.

It was shown that discretising the joints in an exact manner has a significant effect on the monotonic behaviour of RC frames [2], whereas based on the findings herein the overall effect on the mechanical behaviour of RC frames under ultimate limit state cyclic loading conditions is even more important. Hence, this numerical finding demonstrates that the use of the beam-column FE, which is usually a numerical method adopted by researchers when studying retrofitted full-scale structures, is not an accurate numerical approach that can capture the overall mechanical behaviour of RC frames under cyclic loading conditions. This is attributed not only to the complex retrofitted section's mechanical behavior, but also to the interaction between the retrofitted and non-retrofitted structural members that are connected to a joint, where the 3D domain of the joint itself affects the final overall mechanical response when this structural configuration is subjected to extreme cyclic loading conditions (see Fig. 26).

It is evident at this point that retrofitting with CFRP sheets does improve the capacity of the initial framing system, especially the overall increase in terms of base shear resistance. Nonetheless, it was found that the ability of the retrofitted framing system to dissipate energy after excessive damage has occurred, was not improved significantly when the frame was retrofitted at the 1st and 2nd floors only. On the other hand, the retrofitting of the RC frame throughout the height was found to increase the capacity and the energy dissipation. In order to increase the energy dissipation significantly, the retrofitting technique of infill RC shear walls is recommended based on the findings shown in Figs.

27 and 28.

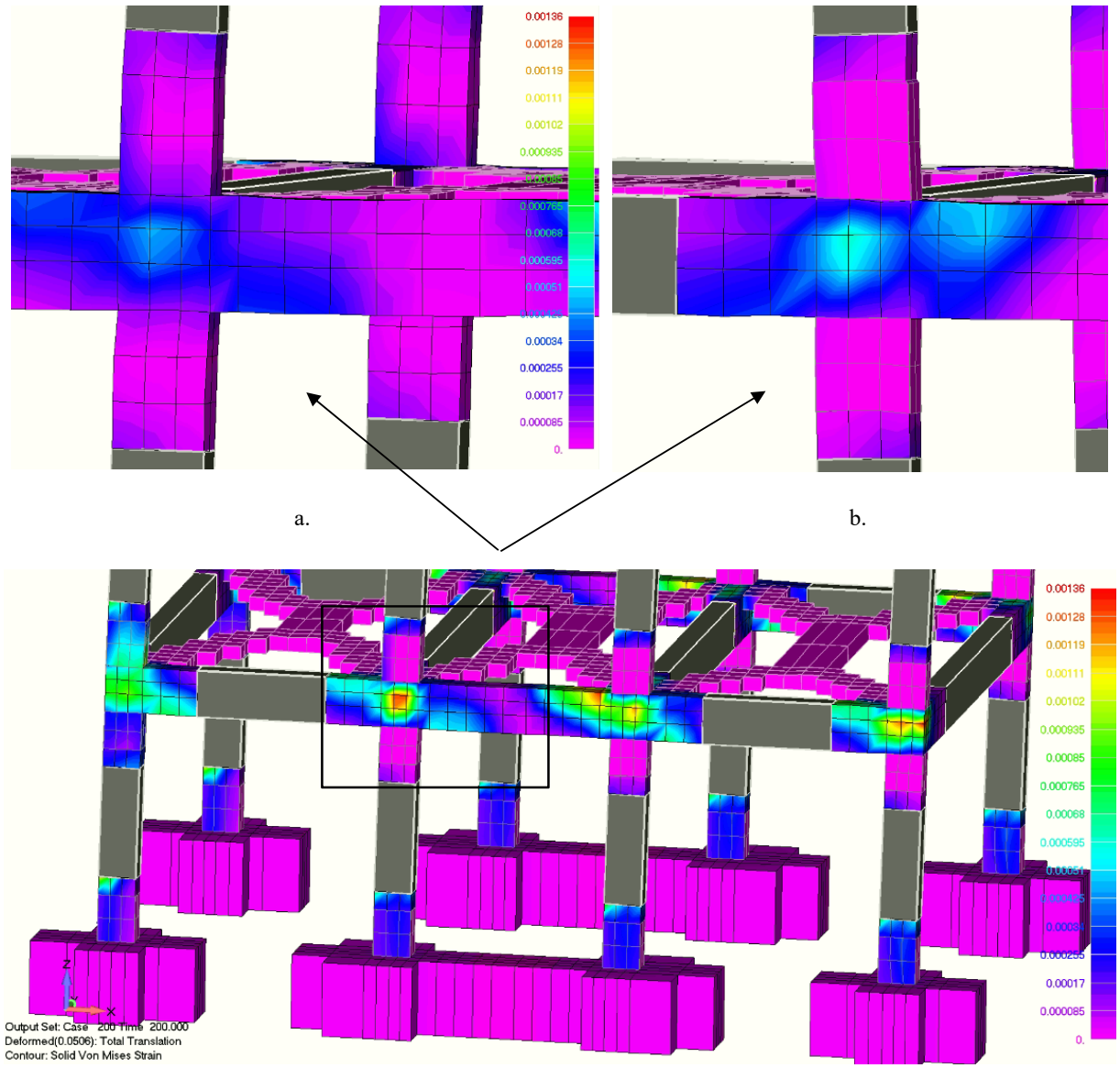

Figure. 26. Model BC505. Von Mises strain contour and deformed shape of (a) δ_x = 23 mm, (b) δ_x = -23 mm and (c) δ_x = 50 mm. Maximum horizontal displacements during the first 2 preparatory cycles.

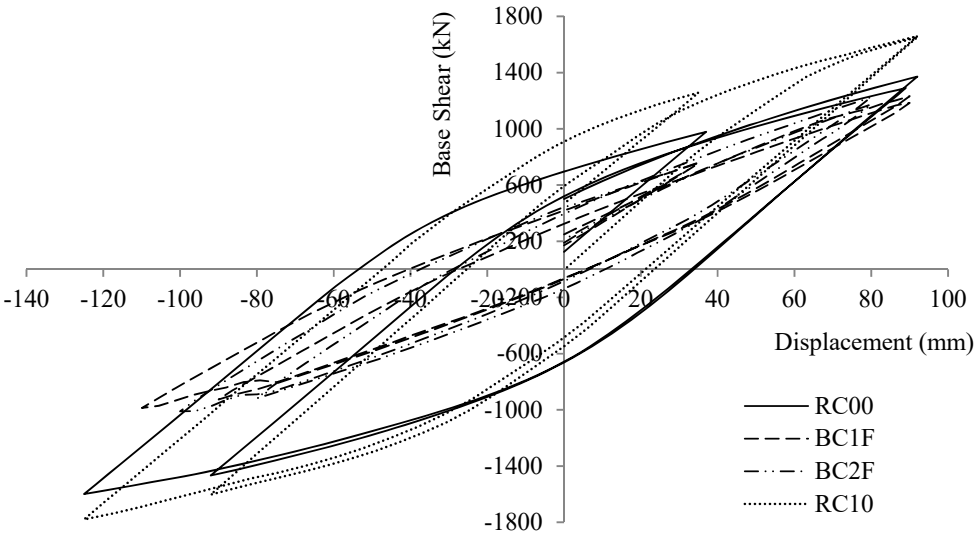

. HYMOD Models RC00, BC1F, BC2F and RC10. Final cycles. Total base shear vs horizontal displacement **Figure.**

27of the top floor.

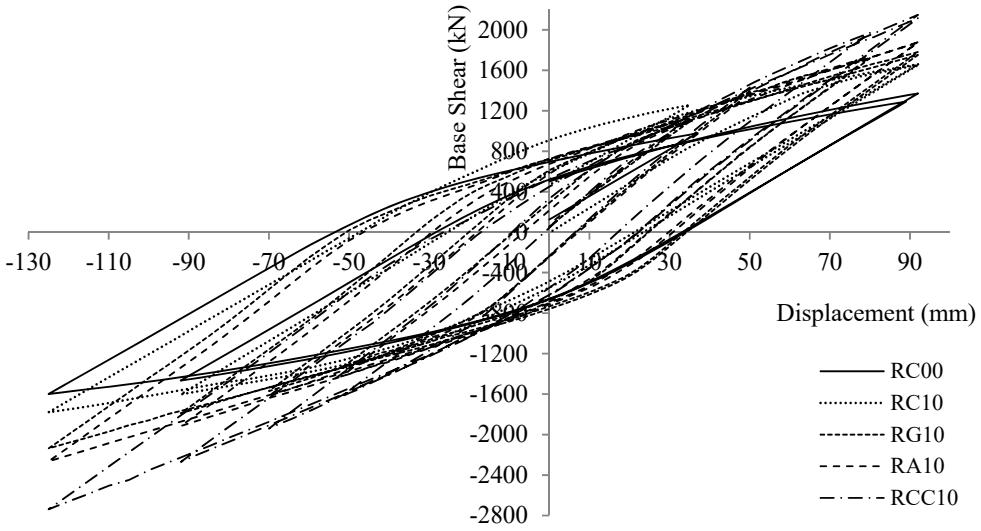

Figure. 28. HYMOD Models RC00, RC10, RG10, RA10 and RCC10. Final cycles. Total base shear vs horizontal displacement of the top floor.

According to Fig. 27, the model that was strengthened by using an infill shear wall throughout the building's height (RC00) placed at both frames (North and South), derived a maximum base shear resistance during the final displacement cycles of 1,599 kN that corresponds to a 1.8 times larger strength compared to the initial frame (BC00). What is also interesting to note herein is the increase of the ability of the strengthened frame to dissipate energy during the entire displacement history that was imposed to the framing system. According to the dissipated energy of model RC00, it was able to

dissipate a total of 818,190 kNm during the entire loading excitation, a magnitude that is 8.5 times larger than that of the initial frame (BC00; 95,749.4 kNm). This illustrated the advantage of adding infill RC shear walls throughout the height of an existing RC building in-terms of strength and energy dissipation increase.

An additional finding that is interesting to mention at this point is the increase of the frame's capacity when a CFRP jacket is added at the base of the two infill RC shear walls (RC10), which resulted in a maximum base shear during the final displacement cycles of 1,779.5 kN. This 11.3% increase in comparison to the RC00 model is attributed to the CFRP sheets added at the edges of the infill RC shear walls as it is illustrated in Fig. 12, where the RC00 model can be seen. The confinement of the RC shear walls' edges due to the CFRP sheets managed to contribute to the overall strength of the RC frame, thus resulting in a higher base shear resistance than the corresponding model without confinement (see Fig. 27).

In the case of the models that assumed Glass (RG10), Aramid (RA10) and Carbon (RCC10) FRP rebars within the infill RC shear walls, the strength increased according to the increase in terms of ultimate stress of the FRP rebar material (see Table 3). It is easy to observe in Fig. 28 that as the ultimate stress of the FRP rebar material increases, the respective maximum base shear capacity of the frame increases. The maximum base shear derived from the parametric investigation was equal to 2,738 kN for the case where CFRP rebars are used (RCC10). This corresponds to 4.8-fold increase in-terms of strength during the final displacement cycles compared to the initial bare RC frame. Fig. 29 show the maximum base shear derived during the final displacement cycles for the buildings that foresaw infill RC shear walls.

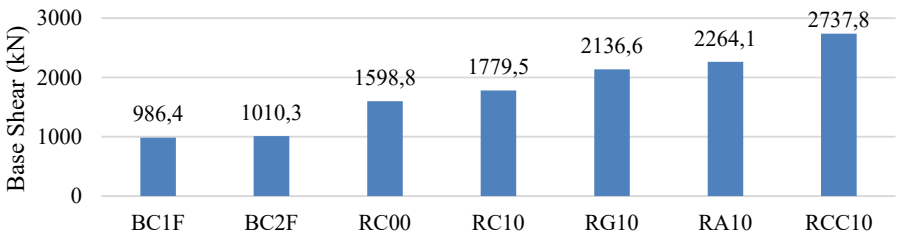

Figure. 29. Maximum base shear derived during the final loading cycles. Retrofitted structures with infill RC shear walls.

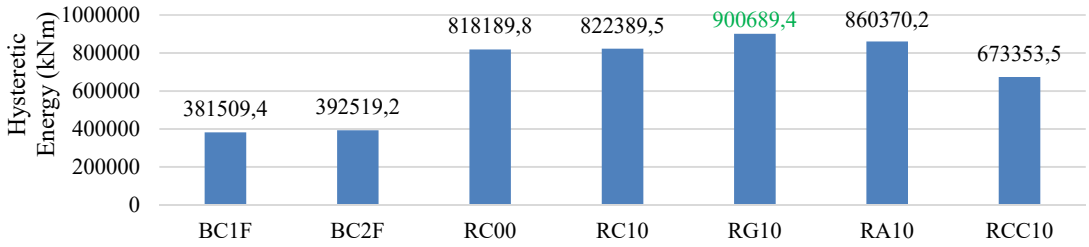

Figure. 30. Hysteretic Energy derived from the full loading history. Retrofitted structures with infill RC shear walls.

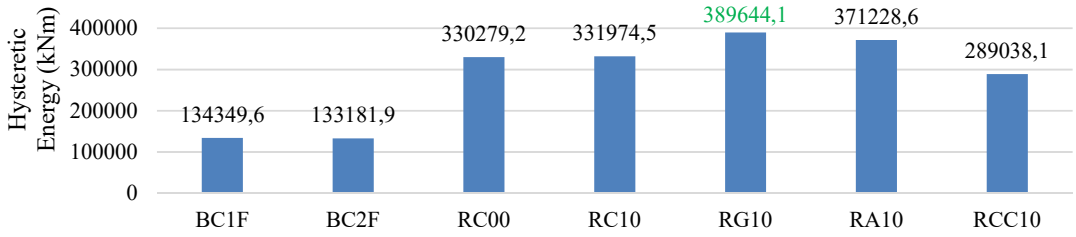

Figure. 31. Hysteretic Energy derived from the final loading cycles. Retrofitted structures with infill RC shear walls.

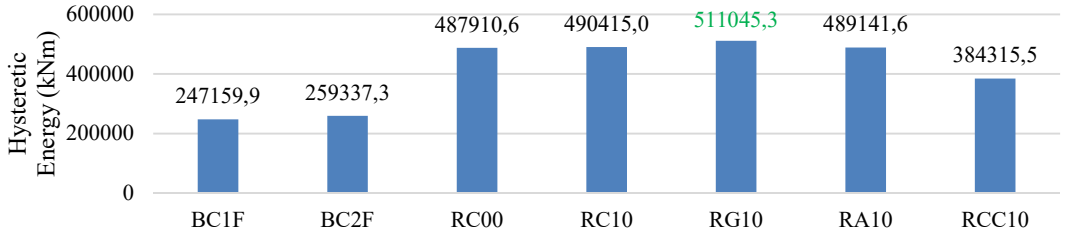

Figure. 32. Hysteretic Energy derived from the preparatory loading cycles. Retrofitted structures with infill RC walls.

Figs. 30-32 show the hysteretic energy that derived during different parts of the loading history as they resulted from the numerical analysis of the frames that were reinforced with infill RC shear walls and different types of rebar materials. It is easy to conclude that in all stages of the cyclic analysis the stiffer material of CFRP rebars found within the infill RC shear wall of model RCC10, derived a lower energy dissipation abilities even though the model's base shear resistance was significantly higher than the rest of the models (RC10, RG10 and RA10). The highest energy dissipation was recorded for the model with its shear walls being reinforced with GFRP rebars. This mechanical behavior is attributed to the Young Modulus of elasticity of the GFRP material that was the lowest out of the four rebar materials that were investigated in this research work. Additionally, it was found that as the Young Modulus of elasticity of the rebars used to construct the infill RC shear walls decreases, the respective energy dissipation increases, while the maximum base shear increase decreases (compared to the initial frame) as the ultimate stress of the rebars decreases.

Finally, it is noteworthy to state at this point that the effect of the infill RC shear walls on the overall mechanical response of the frame does not only contribute to the increase of the energy dissipation and the maximum base shear, but also affects the level of the expected capacity deterioration. Based on the numerical findings, the use of the infill RC shear walls managed to significantly decrease the losses in terms of strength during the final displacement cycles. This phenomenon is attributed to the stiffness of the infill RC shear walls that affect the overall mechanical behaviour of the frame, where this retrofitting technique was found to provide with additional translational support to the frame, allowing the development of resisting mechanisms that are not affected by the accumulated damage that occur at the beam-column joints. For the case of the 4-storey RC frame, the number of beam-column joints prior to the introduction of the infill RC shear walls was 32, whereas the construction of the walls filled the spans and covered the internal beam-column joints shown in Fig. 26, throughout the building height. Therefore, the beam-column joints that remained were the 16 beam-column joints located at the edges of the RC frame.

5.2 Cost-Effectiveness of Interventions

According to the intervention strategy adopted to strengthen the framing system of a RC structure, the overall cost and the final safety level derive accordingly. As discussed above, the type of the implemented intervention can achieve the improvement of the frame's strength (maximum capacity of the frame) and also affect its ductility, therefore, the ability of the frame to dissipate energy. The use of CFRP sheets or infill RC shear walls determine the level of increase in terms of strength and energy dissipation of the frame, but at the same time have a different overall implementation cost. In this section a cost-effectiveness is performed according to the numerical findings presented in section 5.1 and the current available intervention costs that apply in Europe. According to the cost indices found in the construction producer price and construction cost indices overview[1] and based on the repair costs presented in [50], the cost of the two understudy repair techniques was adjusted and are given in Table 4.

[1] https://ec.europa.eu/eurostat/statistics-explained/index.php/Construction_producer_price_and_construction_cost_indices_overview

Table 4. Adjusted repair costs according to prices in Italy, Abruzoo region given in [50].

	Strengthening strategy	Italy (Abruzzo region)
1	CFRP	400 €/m^2/n^o of layer
2	RC shear walls	4150 €/m^3
3	RC shear walls with GFRP*	4650 €/m^3
4	RC shear walls with AFRP*	5430 €/m^3
5	RC shear walls with CFRP*	5430 €/m^3

*Cost that accounts for the increase of the respective FRP rebar material not reported in [50].

It is important to state at this point that the prices and their corresponding variations through time change significantly[2] (within Europe and internationally) thus the development of an optimum building retrofit cost report that assumes any type of strengthening strategy should be performed on a project-to-project basis. This section has as a main objective to illustrate for the first time the importance of using state-of-the-art numerical models to assess the retrofitting strategy based on the overall capacity increase in terms of base shear and dissipation energy based on an ultimate limit state cyclic loading history. Thus, the use of an approximate average retrofit cost is adopted herein. Furthermore, Italy's property and construction material prices represent an average when comparing costs of housing and construction in Europe[3], hence it is adopted herein during the cost estimations.

It is also important to state here that according to [50] the cost of crack injections, sand blasting, primer, putty, demolition and reconstruction of partitions and partition paintings are included when the CFRP jacketing method is used, whereas the cost of rebars arrangement, formwork, concrete casting, foundation strengthening, demolition and reconstruction of partitions, partition paintings and check or restoration of all the systems (water supply, electric installation, etc.) are included in the infill RC shear wall retrofitting method (see Table 3). Furthermore, it must be noted herein that the indirect costs and financial gains when using a corrosive-resistant material such as G-, A- and C-FRP for the rebars found within the infill RC shear walls are not accounted for in Table 4. The cost of

[2] https://assets.publishing.service.gov.uk/government/uploads/system/uploads/attachment_data/file/776136/19-cs2_-_Construction_Building_Materials_-_Commentary_January_2019.pdf
[3] https://www.globalpropertyguide.com/Europe/Italy/square-meter-prices

implementing infill RC shear walls with G-, A- and C-FRP rebars was computed by using the increase in-terms of price when using the composite material instead of standard steel.

Fig. 33 shows the retrofitting cost for each model according to the assumed strengthening strategy and the unit costs of each retrofitting method presented in Table 4. It can be observed that model BC515 that foresees the retrofitting of all columns and beams with 5 layer CFRP sheets, derived the highest cost, whereas the models that foresee the use of infill RC shear walls follow next. Models that use infill RC shear walls with FRP rebars (Aramid and Carbon) derived the highest cost out of all models with infill RC shear walls.

Estimating the overall cost of implementing the different interventions is important but in order to determine the actual cost-efficiency of each proposed retrofitting strategy, the cost has to be compared to the overall mechanical enhancement that each retrofitting strategy achieves based on the results presented in section 5.1. Table 5 provides with a first analysis of the numerically derived maximum base shear recorded during the final cycles of the imposed cyclic loading history, where the overall strength increase is expressed as a percentage of the initial derived strength, where the cost of increasing the initial base shear of the initial frame by 1% (model BC00) is given as well. Table 6 shows the corresponding results for the preparatory loading cycles.

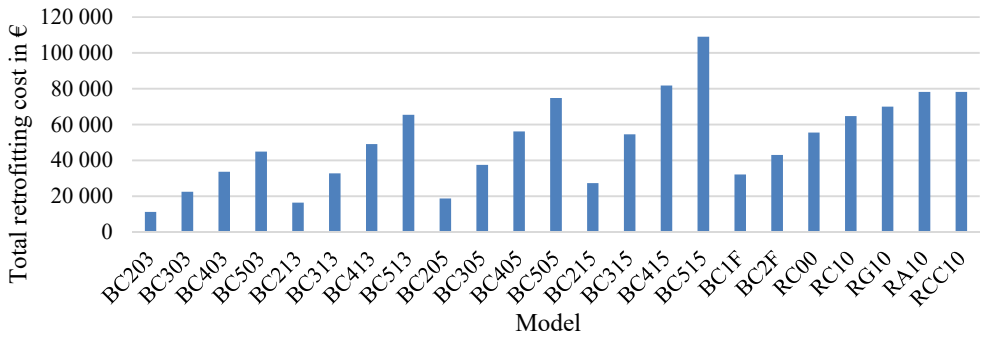

Figure. 33. Total retrofitting cost of each strengthening strategy implemented to the under-study models.

One of the most interesting findings that derives from Table 5 and 6 is the damage that the owner will suffer in the long run if they adopt the retrofitting strategy of models BC205 and BC215. Based on the results given in Table 5, these two models illustrate a mechanical behaviour that derives a slightly lower base shear resistance compared to the initial framing system of model BC00 during the

final loading cycles. Table 6 shows the respective maximum derived base shear values during the preparatory loading cycles, where it can be seen for the two models, BC205 and BC215, the respective increase of the base shear was 3.7% and 2%, respectively. Furthermore, the corresponding increase of the base shear during the first loading cycle was found to be equal to 2.9% and 3.1%, respectively (see Table 7).

Therefore, based on these numerical findings, it is evident that the two retrofitted models manage to increase the overall base shear of the frame during the 1st loading cycle (BC205 → 2.9% and BC215 → 3.1%), whereas as the cyclic loading analysis continues the developed damage and the strain concentrations evolve and derive a 3.7% and 2% increase of the base shear, respectively, during the 5th loading cycle (δ_x = 108 mm). As the nonlinear cyclic analysis was performed beyond the 5th loading cycle, the deterioration of the two models and the damage concentrations led them to derive a lower base shear resistance due to the mechanical phenomenon described in Section 5.1 (see also Fig. 26). Damage concentrations within the joint due to the increased stiffness and strength of the retrofitted column and beam sections forced the non-retrofitted structural members to develop additional damage that eventually led to a lower overall frame resistance during the final loading cycles. Therefore, even though initially the two retrofitted models (BC205 and BC215) exhibited a higher base shear resistance in comparison to the initial frame (BC00), they eventually derived a lower resistance during the final loading cycles. This illustrates the importance of accounting for the exact geometry of the frame that includes the joints and the 3D representation of all structural members of the frame. The accurate representation and discretization of the retrofitting method in combination with the accurate modeling of the damage accumulation for both steel and concrete domains, reveals the overall mechanical response of the retrofitted frame that, as was shown herein, is not always a positive one. This numerical finding also shows that a simple push-over analysis can lead to the wrong conclusions when assessing the overall effect of a retrofitting strategy.

Table 5. Maximum base shear resistance during the final loading cycles. Retrofitting cost and cost for increasing the overall structural strength by 1%.

	Model	Max Base Shear Final Cycles $V_{Rk,max}$ (kN)	Normalized $\frac{V_{Rk,max}}{V_{BC00,Rk,max}}$	Overall Increase $\frac{V_{Rk,max}}{V_{BC00,Rk,max}} \cdot 100 - 100$ (%)	Retrofitting Cost (€)	Cost to increase the strength by 1%
1	BC00	571	1.000	-	-	-
2	BC203	582	1.018	1.8	11,232	6,201
3	BC303	632	1.106	10.6	22,464	2,119
4	BC403	674	1.181	18.1	33,696	1,866
5	BC503	813	1.423	42.3	44,928	1,062
6	BC213	574	1.005	0.5	16,362	33,038
7	BC313	644	1.128	12.8	32,724	2,559
8	BC413	748	1.309	30.9	49,086	1,588
9	BC513	881	1.543	54.3	65,448	1,206
10	BC205	563	0.986	-1.4	18,720	-13,515
11	BC305	622	1.088	8.8	37,440	4,231
12	BC405	676	1.184	18.4	56,160	3,059
13	BC505	1,100	1.926	92.6	74,880	809
14	BC215	529	0.925	-7.5	27,270	-3,649
15	BC315	581	1.017	1.7	54,540	31,762
16	BC415	651	1.140	14.0	81,810	5,850
17	BC515	1,142	2.000	100.0	109,080	1,091
18	BC1F	986	1.727	72.7	32,086	442
19	BC2F	1,010	1.769	76.9	42,980	559
20	RC00	1,599	2.799	179.9	55,527	309
21	RC10	1,779	3.115	211.5	64,767	306
22	RG10	2,137	3.740	274.0	70,017	256
23	RA10	2,264	3.963	296.3	78,207	264
24	RCC10	2,738	4.793	379.3	78,207	206

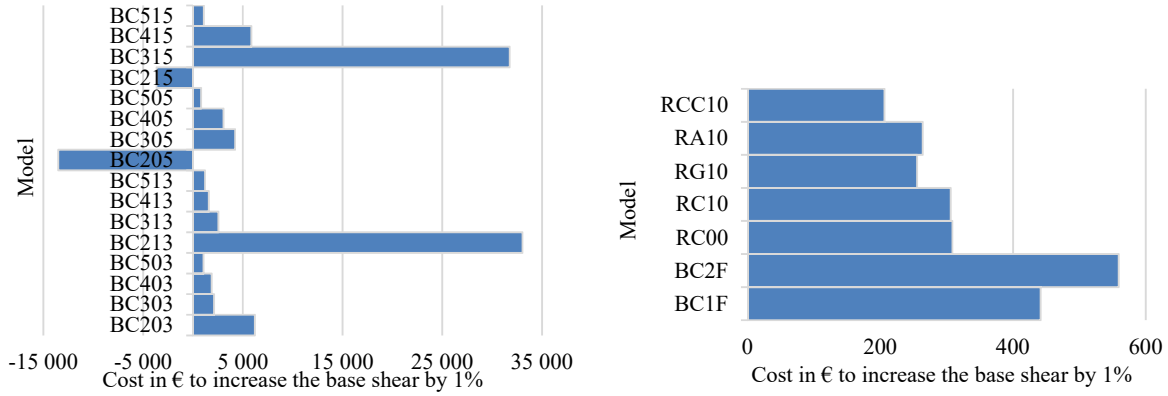

Figure. 34. Cost to increase the base shear by 1% based on the different retrofitting applied. Final loading cycles.

The above finding can be seen as well for the case of the two models BC1F and BC2F, where infill RC shear walls were placed at the 1st floor and at the 1st-2nd floors of the initial frame, respectively. Even though the two models exhibit a significant increase during the initial cycle and the preparatory cycles (Tables 6 and 7), during the final cycles the two models are found to have a larger base shear strength decrease than expected. This is attributed to the non-retrofitted structural member damage accumulation found at the floors above the infill RC shear walls [3].

Furthermore, Tables 5 to 7 show that the cost-effectiveness of each retrofitting strategy varies according to the implementation cost and the relevant strength increase. According to the analysis of the numerically derived data, it is evident that even though the use of CFRP jacketing is overall a less expensive retrofitting method to be implemented, the use of infill RC shear walls derives a more cost-effective solution. Based on Table 5 and Fig. 34, model RCC10 that foresees the use of infill RC shear walls with CFRP rebars derives a cost of 206 € for increasing the base shear resistance of the initial frame by 1% during the final loading cycles. Following this optimum retrofitting strategy, is model RG10 with 256 € and model RA10 with 264 €.

Table 6. Maximum base shear resistance during the preparatory loading cycles. Retrofitting cost and cost to increase the overall structural strength by 1%.

	Model	Max Base Shear Prep. Cycles $V_{Rk,max}$ (kN)	Normalized $\frac{V_{Rk,max}}{V_{BC00,Rk,max}}$	Overall Increase $\frac{V_{Rk,max}}{V_{BC00,Rk,max}} \cdot 100 - 100$ (%)	Retrofitting Cost (€)	Cost to increase the strength by 1%
1	BC00	746	1.000	-	-	0
2	BC203	765	1.025	2.5	11,232	4,558
3	BC303	790	1.058	5.8	22,464	3,845
4	BC403	833	1.116	11.6	33,696	2,907
5	BC503	964	1.291	29.1	44,928	1,543
6	BC213	771	1.033	3.3	16,362	4,973
7	BC313	795	1.065	6.5	32,724	5,040
8	BC413	843	1.130	13.0	49,086	3,789
9	BC513	1,033	1.385	38.5	65,448	1,702
10	BC205	774	1.037	3.7	18,720	5,013
11	BC305	802	1.075	7.5	37,440	5,022
12	BC405	881	1.180	18.0	56,160	3,117
13	BC505	1,230	1.648	64.8	74,880	1,156
14	BC215	762	1.020	2.0	27,270	13,336
15	BC315	815	1.091	9.1	54,540	5,968
16	BC415	870	1.166	16.6	81,810	4,940
17	BC515	1,289	1.727	72.7	109,080	1,501
18	BC1F	2,179	2.919	191.9	32,086	167
19	BC2F	2,212	2.964	196.4	42,980	219
20	RC00	2,239	3.000	200.0	55,527	278
21	RC10	2,514	3.368	236.8	64,767	273
22	RG10	2,580	3.457	245.7	70,017	285
23	RA10	2,690	3.604	260.4	78,207	300
24	RCC10	2,775	3.719	271.9	78,207	288

A general trend based on Tables 5 to 7 and Fig. 34, derives from the fact that the CFRP jacket retrofitting is becoming more cost-efficient as the number of retrofitted floors increases. Models BC503, BC513, BC505 and BC515, derived the lowest costs out of all of the CFRP sheet retrofitted models. BC505 that foresees the retrofitting of all columns of the frame with 5 layers of CFRP sheets derived a 1,156 € per 1% of base shear strength increase (Table 6) followed by the BC515 model that assumes all frame members to be retrofitted with 5 layers of CFRP sheets. Even though the BC515 foresaw for more structural members to be retrofitted with CFRP sheets and derived a higher overall mechanical frame enhancement in comparison to the BC505, model BC505 managed to derive a more optimal cost in terms of overall base shear resistance. The same finding derived from the comparison of the models BC503 and BC513, where the computed cost to increase the base shear by 1% was 1,543 € and 1,702 €, respectively.

Analyzing the mechanical response of RC retrofitted frames in-terms of their overall base shear resistance increase is an acceptable key performance indicator, especially when using nonlinear static cyclic analysis for the assessment of the retrofitting strategy. Nevertheless, an earthquake excitation is an event that will not only test a structure in-terms of strength but also in-terms of its ability to dissipate energy. Therefore, the ability of a retrofitted RC structure is also of significant importance when assessing the overall mechanical response enhancement due to a specific retrofitting design. Table 8 shows the dissipated energy of all retrofitting strategies based on the numerical investigation performed on the final loading cycles.

Table 7. Maximum base shear resistance during the first loading cycle. Retrofitting cost and cost to increase the overall structural strength by 1%.

	Model	Max Base Shear 1st Cycle $V_{Rk,max}$ (kN)	Normalized $\frac{V_{Rk,max}}{V_{BC00,Rk,max}}$	Overall Increase $\frac{V_{Rk,max}}{V_{BC00,Rk,max}} \cdot 100 - 100$ (%)	Retrofitting Cost (€)	Cost to increase the strength by 1%
1	BC00	299	1.000	-	-	0
2	BC203	301	1.008	0.8	11,232	14,893
3	BC303	306	1.025	2.5	22,464	9,103
4	BC403	314	1.052	5.2	33,696	6,501
5	BC503	324	1.085	8.5	44,928	5,311
6	BC213	303	1.013	1.3	16,362	12,578
7	BC313	312	1.044	4.4	32,724	7,518
8	BC413	324	1.086	8.6	49,086	5,716
9	BC513	338	1.131	13.1	65,448	5,014
10	BC205	307	1.029	2.9	18,720	6,560
11	BC305	323	1.081	8.1	37,440	4,616
12	BC405	350	1.171	17.1	56,160	3,288
13	BC505	383	1.282	28.2	74,880	2,660
14	BC215	308	1.031	3.1	27,270	8,871
15	BC315	325	1.089	8.9	54,540	6,112
16	BC415	355	1.188	18.8	81,810	4,360
17	BC515	387	1.296	29.6	109,080	3,688
18	BC1F	741	2.481	148.1	32,086	217
19	BC2F	746	2.496	149.6	42,980	287
20	RC00	756	2.530	153.0	55,527	363
21	RC10	760	2.543	154.3	64,767	420
22	RG10	898	3.008	200.8	70,017	349
23	RA10	919	3.077	207.7	78,207	377
24	RCC10	999	3.344	234.4	78,207	334

Based on the results shown in Table 8 and Fig. 35, only model BC303 did not manage to derive a dissipated energy larger than that of the initial model BC00 during the final loading cycles. The reason why this retrofitting strategy derived a lower energy dissipation in comparison to model BC00 is attributed to the internal stress redistribution during the preparation cycles that led to a decreased performance during the final loading cycles, as discussed in Section 5.1. Therefore, in-terms of cost-effectiveness and energy dissipation, this retrofitting strategy (BC303) is found to be the worst. Additionally, the model RC10 was found to be the optimum retrofitting strategy in-terms of cost-effectiveness related to energy dissipation enhancement (cost to enhance the energy dissipation ability of the initial frame by 1% equal to 70 €). It is also easy to observe that the retrofitted frames that assume infill RC shear walls are significantly more cost-effective in comparison to the CFRP sheet retrofitted frames. This finding is attributed to the ability of the infill RC shear walls to dissipate energy during a seismic event and the inability of the applied CFRP jacketing that did not foresee the complete joint confinement. The mechanical behaviour and modeling of RC substructures and their corresponding hysteretic behaviour, after full CFRP sheet retrofitting is performed, can be found in [55].

It is evident at this point that the equation that will eventually determine the most cost-effective retrofitting strategy should account for both base shear and energy dissipation enhancement compared to the initial frame mechanical response. Furthermore, the proposed relationship between cost-effectiveness, retrofitting cost and structural response enhancement has to account for the ability of the structure to resist to the maximum expected seismic force, whereas its ability to dissipate energy has to be accounted for as well.

Table 8. Dissipated energy during the final loading cycles. Retrofitting cost and cost to increase the hysteretic performance by 1%.

	Model	Dissipated Energy E_i (kNm)	Normalized E_i / E_{BC00}	Overall Increase Normalized x 100 - 100 (%)	Retrofitting Cost (€)	Cost to increase the dissipated energy by 1%
1	BC00	38,112	1.000	-	-	-
2	BC203	41,372	1.086	8.6	11,232	1,313
3	BC303	35,741	0.938	-6.2	22,464	-3,611
4	BC403	40,660	1.067	6.7	33,696	5,040
5	BC503	44,221	1.160	16.0	44,928	2,803
6	BC213	44,083	1.157	15.7	16,362	1,044
7	BC313	44,209	1.160	16.0	32,724	2,045
8	BC413	42,818	1.123	12.3	49,086	3,975
9	BC513	45,802	1.202	20.2	65,448	3,244
10	BC205	41,630	1.092	9.2	18,720	2,028
11	BC305	51,123	1.341	34.1	37,440	1,097
12	BC405	74,821	1.963	96.3	56,160	583
13	BC505	70,416	1.848	84.8	74,880	883
14	BC215	39,406	1.034	3.4	27,270	8,033
15	BC315	44,294	1.162	16.2	54,540	3,362
16	BC415	59,269	1.555	55.5	81,810	1,474
17	BC515	58,377	1.532	53.2	109,080	2,051
18	BC1F	134,350	3.525	252.5	32,086	127
19	BC2F	133,182	3.494	249.4	42,980	172
20	RC00	330,279	8.666	766.6	55,527	72
21	RC10	389,644	10.224	922.4	64,767	70
22	RG10	389,644	10.224	922.4	70,017	76
23	RA10	371,229	9.740	874.0	78,207	89
24	RCC10	289,038	7.584	658.4	78,207	119

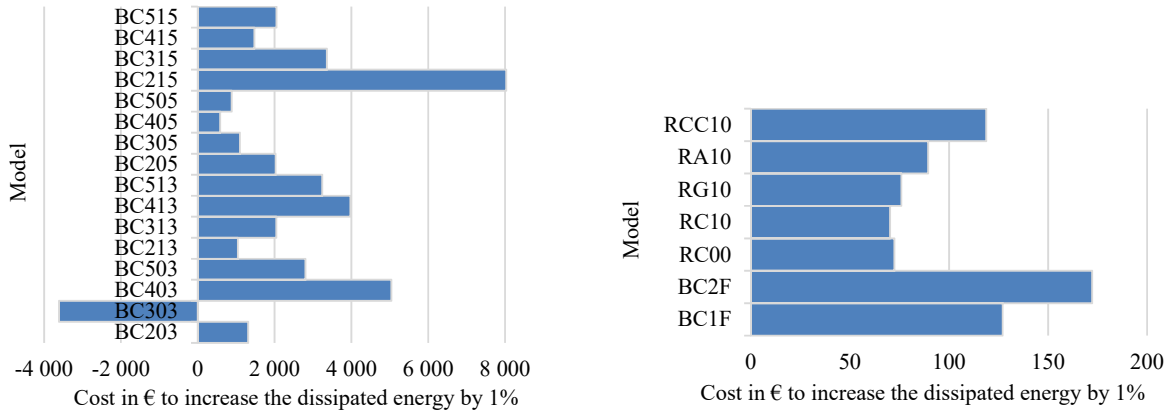

Figure. 35. Cost to increase the dissipated energy by 1% for different retrofitting strategies. Final loading cycles.

The following relationship is proposed here to determine the optimum retrofitting strategy based on a nonlinear cyclic static loading investigation that foresees the calculation of an optimum retrofitting cost factor O_{RCF}:

$$O_{RCF.} = \left[\psi_S \left(\frac{\mathrm{V_{Rk,i,max}}}{\mathrm{V_{Ini.,Rk,max}}} - 1\right) + \psi_D \left(\frac{\mathrm{E_i}}{\mathrm{E_{Ini}}} - 1\right)\right] \cdot n_{CR} > 0, where, n_{CR} = \frac{C_{R,max}}{C_{R,i}} \quad (13)$$

where, $\mathrm{V_{Rk,i,max}}$ the maximum base shear strength in kN of the i-th retrofitting strategy, $\mathrm{V_{Ini.,Rk,max}}$ the maximum base shear strength in kN of the initial frame, $\mathrm{E_i}$ is the energy dissipation of the i-th retrofitting strategy during the under-study loading cylces and $\mathrm{E_{Ini}}$ the corresponding energy dissipation in kNm of the initial frame without retrofitting. Parameters $C_{R,i}$ and $C_{R,max}$ are the retrofit cost of the i-th model and the model with the maximum retrofit cost, repsectively. Constant parameters ψ_S and ψ_D, represent the importance factors of strength and energy dissipation enhancement, respectively, where these parameters are set by the engineer according to the desired overall response enhancement of the initial frame. These two factors should satisfy the following conditions:

$$\psi_S + \psi_D = 1 \quad and \quad 0 \leq (\psi_S, \psi_D) \leq 1 \quad (14)$$

Furthermore, in the case where the proposed optimum retrofitting cost factor is smaller than 0, the proposed retrofitting strategy does not only affect in a negative manner some or all of the mechanical seismic resistance characteristics of the structure, but it also adds negative cost to the expected overall economic performance of the structure. Therefore, the owner will suffer not only the cost of

implementing the retrofitting but also will require to suffer increased financial damage due to increased repair costs due to a future seismic event when compared to the costs that the owner would have to undertake if the frame was left without any retrofitting. By assuming herein that $\psi_S = 70\%$ and $\psi_D = 30\%$, Table 9 was developed according to the numerical data obtained during the final loading cycles (see Tables 4 and 7). Based on the at hand structure, it derives that the RA10 model's retrofitting strategy derives the optimum cost-effectiveness, whereas BC215 exhibits the worst with a negative 0.011 factor. It is also interesting to note that from the CFRP sheet strengthened models BC515 derived the optimum cost-effectiveness for the assumed importance factors.

To further investigate the proposed equation, the importance factor ψ_S is set to 50% and 30%, repsectively, where the corresponding Tables 9 and 10 were developed and shown herein. It is easy to observe from Table 10 that the modification of the importance factors derived the same optimum and worst retrofitting strategy, while for the case of $\psi_S = 30\%$ and $\psi_D = 70\%$ (see Table 11) the less effective retrofitting strategy shifts to model BC303, which was the model that derived the lowest energy dissipation performance (see Table 8).

It is also important to note here that by assuming a $\psi_S = 100\%$ the optimum retrofitting strategy is that of RCC10 with O_{RCF} = 2.719, which was the model that derived the highest base shear increase. Additionally, the O_{RCF} factor becomes equal to 0.916 for the RC00 model (infill RC shear walls throughout the height of the building with steel rebars), where the respective factor for model BC515 is equal to 1.00 (see Table 12). Therefore, when the strength increase is the main goal when selecting the most cost-effective retrofitting strategy, the CFRP sheet configuation used in model BC515 becomes more cost-effective than the use of infill RC shear walls (model RC00).

In addition, the selection of an optimum retrofitting strategy based on a restrictive budget can be easily performed herein by removing the out of budget retrofitting strategies from the selection process. Table 13 shows the corresponding O_{RCF} factors for the retrofitting strategies that lie within a maximum retrofit budget of 35,000 € for the case of $\psi_S = 90\%$ and $\psi_D = 10\%$ (case where the strength increase is more important than the corresponding hysteretic enhancement). Furthermore, if

we assume that for different reasons the use of infill RC shear walls is not feasible (i.e. due to the presence of important openings), then the retrofit strategy implemented in model BC403 is the optimum choice with an overall cost of 33,969 € (see Table 5). Furthermore, the proposed factor can be used in combination with other expected costs such as economic losses due to casualties and injuries, property unavailability, maintenance costs, etc., to further investigate any retrofitting strategy's life-cycle cost optimization and form a crucial decision tool during cost-benefit analysis [48, 49, 50, 61 and 62].

Table 9. Optimum retrofitting cost factor O_{RCF} for the case of $\psi_S = 70\%$ and $\psi_D = 30\%$.

	Model	O_{RCF}		Model	O_{RCF}		Model	O_{RCF}
1	BC00	0.0	9	BC513	0.264	17	BC515	0.859
2	BC203	0.004	10	BC205	0.003	18	BC1F	0.372
3	BC303	0.011	11	BC305	0.056	19	BC2F	0.507
4	BC403	0.045	12	BC405	0.215	20	RC00	1.812
5	BC503	0.142	13	BC505	0.620	21	RC10	2.522
6	BC213	0.008	**14**	**BC215**	**-0.011**	22	RG10	3.007
7	BC313	0.041	15	BC315	0.030	**23**	**RA10**	**3.367**
8	BC413	0.114	16	BC415	0.198	24	RCC10	3.320

Table 10. Optimum retrofitting cost factor O_{RCF} for the case of $\psi_S = 50\%$ and $\psi_D = 50\%$.

	Model	O_{RCF}		Model	O_{RCF}		Model	O_{RCF}
1	BC00	0.0	9	BC513	0.223	17	BC515	0.766
2	BC203	0.005	10	BC205	0.007	18	BC1F	0.478
3	BC303	0.005	11	BC305	0.074	19	BC2F	0.643
4	BC403	0.038	12	BC405	0.295	20	RC00	2.409
5	BC503	0.120	13	BC505	0.609	21	RC10	3.366
6	BC213	0.012	**14**	**BC215**	**-0.005**	22	RG10	3.840
7	BC313	0.043	15	BC315	0.045	**23**	**RA10**	**4.196**
8	BC413	0.097	16	BC415	0.261	24	RCC10	3.720

Table 11. Optimum retrofitting cost factor O_{RCF} for the case of $\psi_S = 30\%$ and $\psi_D = 70\%$.

	Model	O_{RCF}		Model	O_{RCF}		Model	O_{RCF}
1	BC00	-	9	BC513	0.182	17	BC515	0.672
2	BC203	0.007	10	BC205	0.010	18	BC1F	0.584
3	**BC303**	**-0.002**	11	BC305	0.091	19	BC2F	0.779
4	BC403	0.031	12	BC405	0.375	20	RC00	3.006
5	BC503	0.099	13	BC505	0.598	21	RC10	4.210
6	BC213	0.017	14	BC215	0.000	22	RG10	4.672
7	BC313	0.045	15	BC315	0.059	**23**	**RA10**	**5.024**
8	BC413	0.081	16	BC415	0.323	24	RCC10	4.120

Table 12. Optimum retrofitting cost factor O_{RCF} for the case of $\psi_S = 100\%$ and $\psi_D = 0\%$.

	Model	O_{RCF}		Model	O_{RCF}		Model	O_{RCF}
1	BC00	-	9	BC513	0.326	17	BC515	1.000
2	BC203	0.002	10	BC205	-0.002	18	BC1F	0.214
3	BC303	0.022	11	BC305	0.030	19	BC2F	0.303
4	BC403	0.056	12	BC405	0.095	20	RC00	0.916
5	BC503	0.174	13	BC505	0.636	21	RC10	1.256
6	BC213	0.001	**14**	**BC215**	**-0.019**	22	RG10	1.759
7	BC313	0.038	15	BC315	0.009	23	RA10	2.125
8	BC413	0.139	16	BC415	0.105	**24**	**RCC10**	**2.719**

A final analysis of the numerical behaviour of the proposed optimum retrofitting cost factor O_{RCF} is performed at this stage to further illustrate the resulted magnitudes of the proposed factor in relation to the selected importance factors ψ_S and ψ_D. Given that the two importance factors (ψ_S, ψ_D) are linearly connected and should always sum to 1 (see Eq. 14), the variation of factor O_{RCF} was computed for different value combinations of (ψ_S, ψ_D) and given in Fig. 33. The graphs for models BC215, BC303, BC515, RC00 and RA10 are provided in this figure, where it is evident that the decision making on whether a retrofitting is the optimum or not, depents not only on the overall retrofit cost in

relation to the strength increase but also on the erergy dissipation enhancement that the retrofit strategy achieves based on the 3D detailed numerical modeling. Additionally, the selesction of the importance factors (ψ_S, ψ_D) that relate to the strength and energy dissipation enhancements, repsectively, are also crucial when deciding what will be the main goals prior to designing the interventions that will be implemented to strengthen the initial framing system.

Table 13. Optimum retrofitting cost factor $\psi_S = 90\%$ and $\psi_D = 10\%$. Overall retrofit cost limitation of 35,000 €.

	Model	O_{RCF}		Model	O_{RCF}
1	BC00	-	6	BC313	1.131
2	BC203	1.025	7	BC205	0.997
3	BC303	1.089	8	BC215	0.936
4	**BC403***	**1.169**	**9**	**BC1F**	**1.907**
5	BC213	1.020			

*Optimum retrofitting strategy in the case where infill RC shear walls is not a feasible solution.

Fig. 36a shows the case of the computed proposed factor O_{RCF} for the cases of models BC215 and BC303, where it is evident that the cost benefit that derives from the strength increase (base shear) due to the CFRP sheets for the case of model BC303 is positive when the importance factor ψ_S is larger than 0.35, while for the case of the model BC215 the retrofitting strategy is economically beneficial if the main goal is to enhance the energy disipation capabilities of the bare frame ($\psi_D > 70\%$). The same phenomenon leads the retrofitting strategy applied in model BC515 to become a more cost-effective option compared to the infill RC shear walls (RC00) when the strength enhancement is the main objective when designing the retrofit system (see Fig. 36b). Before moving to the next and final section of this manuscript, it is noteworthy to say that the total size of the output files that were generated from this numerical investigation was approximately 1.2 Tb.

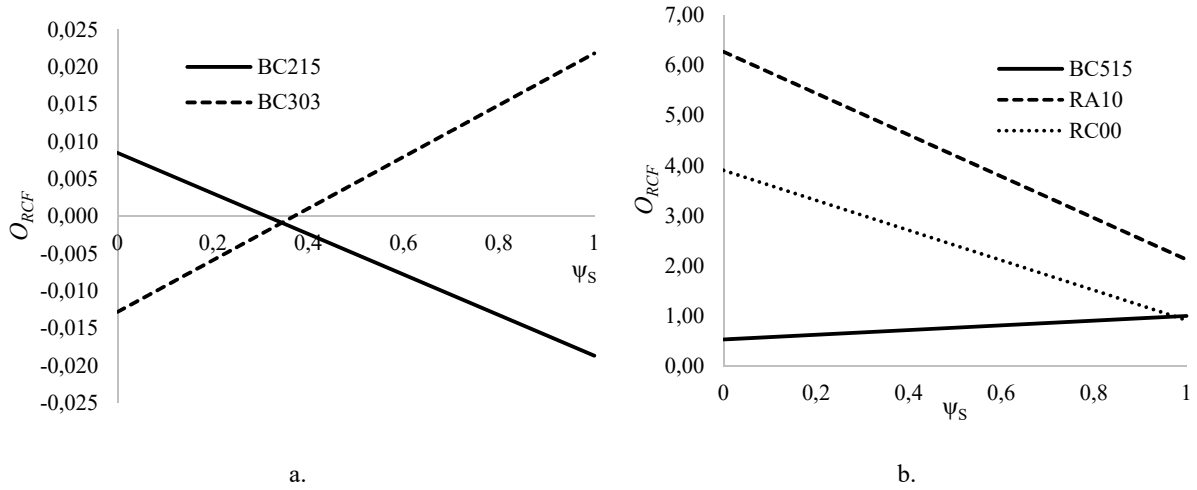

a. b.

Figure. 36. O_{RCF} factor vs ψ_S. Graphs based on the mechanical response of models (a) BC215 and BC303; (b) BC515, RC00 and RA10.

6. Conclusions and Future Work

Based on the numerical findings presented in this section, the proposed modeling method was found to have the ability to capture experimental results of RC joints that are strengthened with CFRP jacketing, where the numerical and experimental data were found to be in a good agreement. Additional numerical verifications can also be found in [55].

The numerical findings presented in this manuscript related to the hysteretic behaviour of the understudy 4-storey RC building that was retrofitted by using different CFRP sheet configurations and infill RC shear walls, indicate that the overall mechanical response of the retrofitted structure is significantly affected not only by the type of retrofitting, but also by the location of the structural members that are selected to be strengthened. The overall computed strength increase and energy dissipation enhancement when the CFRP sheets were used to strengthen the columns and beams of the building revealed that the retrofitting strategies that foresaw the strengthening of at least a 75% of the building's floors (starting from the foundation level and moving towards the roof) derived the highest improvement in terms of structural response.

Additionally, it was found that for cases where the structure was reinforced only at the ground floor level by strengthening the columns alone, the structure's hysteretic behaviour and for the cases of models BC205 and BC215 the cyclic strength resistance during the final loading cycles could be

negatively affected. This phenomenon is attributed to the damage mitigation at the beam-column joints, where the strengthened columns exhibited an increased capacity in comparison to the joint domain that is usually not discretized and modelled when beam-column finite elements are used to simulate retrofitted RC structures. In the case where hexahedral elements combined with embedded rebar elements are used to discretize the shear dominated structural members of the RC frame in an exact manner, all main physical phenomena that take place within the joints of a structure can be realistically captured during an ultimate limit state cyclic loading history, thus in this case reveal cases where the under-study retrofitting strategy will lead to a premature failure or a decreased hysteretic performance due to the accumulated damage at the non-retrofitted structural members that are connected to the strengthened members. This is a phenomenon that is neglected when beam-column finite elements are used to perform the numerical discretization and analysis of RC structure.

Developing decision-making tools by assessing the life-cycle cost-effectiveness of a retrofitting strategy is of great importance and should be based on objective numerical models that can realistically predict the nonlinear mechanical behaviour of the bare and retrofitted RC frames. For this reason, a new optimum retrofitting cost factor is proposed in this research work that uses the base shear force enhancement and the increase in terms of energy dissipation of the retrofitted structure compared to the initial RC structure. The numerically obtained base shear and energy dissipation that derive from the ultimate limit state nonlinear static cyclic analysis are used to determine the optimum cost-effectiveness of the designed retrofitting strategy, where the decision on the weight of each enhancement is determined by defining two importance factors (ψ_S, ψ_D) that are directly associated with the respective computed enhancement of strength and energy dissipation. The newly proposed optimum retrofitting cost factor O_{RCF} was utilized in this work in determining the most cost-effective retrofitting strategy.

Based on the numerical investigation, the most cost-effective retrofitting method when the objective was to achieve a maximum strength enhancement was the use of infill RC shear walls reinforced with CFRP rebars. For the case where the objective was to enhance both strength and energy dissipation in a balanced manner (case where $\psi_S = 50\%$ and $\psi_D = 50\%$), model RA10 was found to

be the optimum retrofit strategy (infill RC shear walls with AFRP rebars). If conventional infill RC shear walls (with steel rebars) are considered then the results for an importance factor $\psi_S \leq 95\%$ indicate that this retrofitting strategy is more cost-effective than the CFRP jacketing method, even when all structural members of the bare frame are retrofitted with CFRP sheets. When the importance factor ψ_S is assumed to be larger than 95% then the CFRP jacketing retrofitted model BC515 becomes a more cost-effective solution. The derived results are based on the assumed CFRP jacketing geometries and pricing adopted for the needs of this study. Therefore, the final conclusions in regards to the most cost-effective retrofitting strategy may vary from country to country.

The use of nonlinear dynamic analysis for the development of a respective optimum retrofitting cost factor O_{RCF} has to be performed in the future to provide with an even more realistic and accurate decision making tool. Finally, the use of the developed technology will be used to perform numerical investigations on retrofitting strategies through models that will account for the soil-structure interaction effect in a realistic manner [63-65].

Acknowledgement

Part of the analysis of the developed large-scale numerical models were performed through the use of a fast PC that was purchased under the financial support received from the Research Development Programme (RDP), year 2019, round No 1, University of Pretoria, under the project titled Future of Reinforced Concrete Analysis (FU.RE.CON.AN.); a research fund awarded to the author in support of his research activities. This financial support is highly acknowledged.

References

[1] Markou, G., Mourlas, Ch. and Papadrakakis, M. (2017), "Cyclic Nonlinear Analysis of Large-Scale Finite Element Meshes Through the Use of Hybrid Modeling (HYMOD)", International Journal of Mechanics, 11(2017), pp. 218-225.

[2] Markou, G., Mourlas, C. and Papadrakakis, M. (2019), "A Hybrid Finite Element Model (HYMOD) for the Non-Linear 3D Cyclic Simulation of RC Structures", International Journal of Computational Methods, 16(1), 1850125, pp. 1-40.

[3] Markou, G., Mourlas, Ch., A. Bark and Papadrakakis, M. (2018), "Simplified HYMOD Non-Linear Simulations of a Full-Scale Multistory Retrofitted RC Structure that Undergoes Multiple Cyclic Excitations – An infill RC Wall Retrofitting Study", Engineering Structures, 176 (2018), pp. 892–916.

[4] CODE OF STRUCTURAL INTERVENTIONS 2012, Earthquake Planning and Protection Organization of Greece (E.P.P.O.), ISBN:978-618-80586-0-6.

[5] Eurocode 8 (2003), Design of structures for earthquake resistance.

[6] Markou, G. and Papadrakakis, M. (2013), "Computationally efficient 3D finite element modeling of RC structures", Computers and Concrete, 12(4), 443–98.

[7] Mourlas Ch., Papadrakakis M. and Markou M., "Accurate and Efficient Modeling for the Cyclic Behavior of RC Structural Members", ECCOMAS Congress, VII European Congress on Computational Methods in Applied Sciences and Engineering, Crete Island, Greece, 5–10 June 2016.

[8] Tedesco, J. W., Stallings, J. M., and El-Mihilmy, M. (1999), "Finite Element Method Analysis of a Concrete Bridge Repaired with Fiber Reinforced Plastic Laminates," Computers and Structures, 72, 379-407.

[9] Arduini, M., Di Tommaso, A., and Nanni, A., "Brittle Failure in FRP Plate and Sheet Bonded Beams," ACI Structural Journal, 94(4), pp. 363-370, 1997.

[10] Kachlakev, D., Miller, T., Yim, S., Chansawat, K. and Tanarat, P., Finite Element Modeling of Reinforced Concrete Structures Strengthened with FRP Laminates, Final Report for the Oregon Department of Transportation Research Group and Federal Highway Administration, 2001.

[11] ANSYS, ANSYS User's Manual Revision 18.0, ANSYS, Inc., Canonsburg, Pennsylvania, 2017, http://www.ansys.com

[12] SAP2000, Integrated Software for Structural Analysis and Design, CSI America, 2017, https://www.csiamerica.com/

[13] Rashid, Y.M. (1968), Ultimate strength analysis of prestressed concrete vessels, Nucl Eng and Des, Vol. 7, pp. 334-344.

[14] Mostofinejad, D. and Talaeitaba, S. B. (2006), "Finite Element Modeling of RC Connections Strengthened with FRP Laminates", Iranian Journal of Science & Technology, Transaction B, Engineering, Vol. 30, No. B1, pp. 21-30.

[15] Godat, A., Neale, K. W. and Labossière, P. (2007), "Numerical Modeling of FRP Shear-Strengthened Reinforced Concrete Beams", Journal of Composites for Construction, ASCE, 11(6), pp. 640-649.

[16] ADINA. (2017), Release Notes, Finite Element Analysis Software, Version 19.3, ADINA R & D, Inc., http://www.adina.com

[17] Koteš, P. and Kotula, P. (2007), "Modeling and strengthening of RC bridges by means of CFRP", International Association of Fracture Mechanics for Concrete and Concrete Structures, FraMCos-6 Catania, Italy, 2007 Proceedings, Paper 08-11.

[18] ATENA (2017), Version 5.4.1, www.cervenka.cz

[19] Ibrahim, A. M. and Mahmood, M. Sh. (2009), "Finite Element Modeling of Reinforced Concrete Beams Strengthened with FRP Laminates", European Journal of Scientific Research,30(4), pp. 526-541.

[20] Chansawat, K., Tanarat, P., Miller, T. H., Yim, S. C. and Kachlakev, D. I. (2009), "FE Models of GFRP and CFRP Strengthening of Reinforced Concrete Beams", Advances in Civil Engineering, volume 2009, pp. 1-13.

[21] Niroomandi, A., Maheri, A., Maheri, M. R. and Mahini, S.S. (2010), "Seismic performance of ordinary RC frames retrofitted at joints by FRP sheets", 32(8), pp. 2326–2336

[22] Young-Min, Y., Ashraf, A. M. and Abdeldjelil, B. F. (2011), "Three-Dimensional Nonlinear Finite-Element Analysis of Prestressed Concrete Beams Strengthened in Shear with FRP Composites", Journal of Composites for Construction, ASCE, 15(6), pp. 896-907

[23] DIANA (2017), Version 10.1, Finite Element Analysis Software, TNO DIANA BV. Delft, Netherlands.

www.dianafea.com

[24] Sinaei, H., Jumaat, M. Z. and Shariati, M. (2011), "Numerical investigation on exterior reinforced concrete Beam-Column joint strengthened by composite fiber reinforced polymer (CFRP)", International Journal of the Physical Sciences, 6(28), pp. 6572-6579.

[25] Shuraim, A. B. (2011), "Efficacy of CFRP configurations for shear of RC beams: experimental and NLFE", Structural Engineering and Mechanics, 39(3), pp. 361-382.

[26] ABAQUS (2017), Version 2017, Finite Element Analysis Software, Dassault Systemes. https://www.3ds.com/products-services/simulia/products/abaqus/latest-release/

[27] El-Hacha, R., Zangeneh, P. and Omran, H. Y. (2012), "Finite Element Modeling of Steel-Concrete Composite Beams Strengthened with Prestressed CFRP Plate", International Journal of Structural Stability and Dynamics, 12(1), pp. 23-51.

[28] Cortés-Puentes, W. L. and Palermo, D. (2012), "Modeling of RC Shear Walls Retrofitted with Steel Plates or FRP Sheets", Journal of Structural Engineering, ASCE, 138(5), pp. 602-612.

[29] Alhaddad, M. S.; Siddiqui, N. A.; Abadel, A. A.; Alsayed, S. H. and Al-Salloum, Y. A. (2012), "Numerical Investigations on the Seismic Behavior of FRP and TRM Upgraded RC Exterior Beam-Column Joints", Journal of Composites for Construction, 16(3), pp. 308-321.

[30] LS-DYNA (2017), Version 971, Finite Element Analysis Software. Livermore Software Technology Corporation, http://www.lstc.com/products/ls-dyna

[31] Elsanadedy, H. M., Al-Salloum, Y. A., Alsayed, S. H. and Iqbal, R. A. (2012), "Experimental and numerical investigation of size effects in FRP-wrapped concrete columns", Construction and Building Materials 29, pp. 56–72.

[32] Elsanadedy, H. M., Almusallam, T. H., Alsayed, S. H. and Al-Salloum, Y. A. (2013), "Flexural strengthening of RC beams using textile reinforced mortar – Experimental and numerical study", Composite Structures, 97, pp.40–55.

[33] Milani, G. and Lourenço, P. B. (2013), "Simple Homogenized Model for the Nonlinear Analysis of FRP-Strengthened Masonry Structures. II: Structural Applications", Journal of Engineering Mechanics, ASCE, 139(1), pp. 77-93.

[34] Anania, L. and D'Agata, G. (2013), "Numerical investigation on a new CFRP technology for the upgrading of the RC framed structures", Conference: ICCEN2014, Asia-Pacific Chemical, Biological & Environmental Engineering Society.

[35] Dalalbashi, A., Eslami, A. and Ronagh, H. R. (2013), "A numerical investigation on the hysteretic behavior of RC joints retrofitted with different CFRP configurations", Journal of Composites for Construction, 17(3), pp. 271-382.

[36] Mahini, S.S. and Ronagh, H.R. (2011), "Web-bonded FRPs for relocation of plastic hinges away from the column face in exterior RC joints", Composite Structures, 93 (2011), pp. 2460–2472.

[37] Hognestad, E., Hanson, N. W. and Mchenry, D. (1955), "Concrete stress distribution in ultimate strength design", American Concrete Institute Journal, 27(4), pp. 455-479.

[38] Gribniak, V., Arnautov, A. K., Kaklauskas, G., Jakstaite, R., Tamulenas, V. and Gudonis, E. (2014), "Deformation Analysis of RC Ties Externally Strengthened with FRP Sheets", Mechanics of Composite Materials, 50(5), pp. 669-676.

[39] Duarte, P., Correia, J. R., Ferreira, J. G., Nunes, F. and Arruda, M. R. T. (2014), "Experimental and numerical study on the effect of repairing reinforced concrete cracked beams strengthened with carbon fibre reinforced polymer laminates", Canadian Journal of Civil Engineering, 41, pp. 222–231.

[40] Nasr, Z. H., Alaa, G. S. and Amal, H. Z. (2015), "Finite element analysis of reinforced concrete beams with opening strengthened using FRP", Ain Shams Engineering Journal, https://doi.org/10.1016/j.asej.2015.10.011

[41] Qapo, M., Dirar, S., Yang, J. and Elshafie, M. Z. E. B. (2015), "Nonlinear finite element modelling and parametric study of CFRP shear-strengthened prestressed concrete girders", Construction and Building Materials, 76, pp. 245–255.

[42] Mrozek, M., Mrozek, D. and Wawrzynek, A. (2015), "Numerical analysis of selection of the most effective configuration of CFRP composites reinforcement of masonry specimens", Composites Part B: Engineering, 70, pp. 189–200.

[43] Mazzucco, G., Salomoni, V. A., Majorana, C. E., Pellegrino, C. and Ceccato, C. (2016), "Numerical investigation of concrete columns with external FRP jackets subjected to axial loads", Construction and Building Materials, 111, pp. 590–599.

[44] Azarm, R., Maheri, M. R. and Torabi, A. (2016), "Retrofitting RC Joints Using Flange-Bonded FRP Sheets", Iranian Journal of Science and Technology, Transactions of Civil Engineering, 41(1), pp 27–35.

[45] Lampropoulos, A.P., Paschalis, S.A., Tsioulou, O.T. and Dritsos, S.E. (2016), "Strengthening of reinforced concrete beams using ultra high performance fibre reinforced concrete (UHPFRC)", Engineering Structures 106, pp. 370–384.

[46] Banjara, N. K. and Ramanjaneyulu, K. (2017), "Experimental and numerical investigations on the performance evaluation of shear deficient and GFRP strengthened reinforced concrete beams", Construction and Building Materials, 137, pp. 520–534.

[47] Reconan FEA v1.00, Finite Element Analysis Software Manual, 2010.

[48] Kappos A.J. and Dimitrakopoulos E.G. (2008), "Feasibility of pre-earthquake strengthening of buildings based on cost-benefit and life-cycle cost analysis, with the aid of fragility curves", Natural Hazards, 45, pp. 33–54.

[49] Chrysostomou C.Z., Kyriakides N., Papanikolaou V.K., Kappos A.J., Dimitrakopoulos E.G., Giouvanidis A.I. (2015), "Vulnerability assessment and feasibility analysis of seismic strengthening of school buildings", Bull Earthq Eng, 13:3809–3840.

[50] Vitiello, U., Asprone, D., Di Ludovico, M. and A. Prota (2016), "Life-cycle cost optimization of the seismic retrofit of existing RC structures", Bull Earthquake Eng, 15(5), pp 2245–2271.

[51] Engen, M., Hendriks, M. A. N., Øverli, J. A., & Åldstedt, E. (2017). Non-linear finite element analyses applicable for the design of large reinforced concrete structures. European Journal of Environmental and Civil Engineering, pp. 1-23.

[52] Markou, G. and Papadrakakis, M. (2015), "A Simplified and Efficient Hybrid Finite Element Model (HYMOD) for Non-Linear 3D Simulation of RC Structures", Engineering Computations, 32 (5), pp. 1477-1524.

[53] Mourlas, Ch., Papadrakakis, M. and Markou, G. (2017), "A Computationally Efficient Model for the Cyclic Behavior of Reinforced Concrete Structural Members", Engineering Structures, 141, pp. 97–125.

[54] Kotsovos, M. D. and Pavlovic, M. N., Structural concrete. Finite Element Analysis for Limit State Design, Thomas Telford, London, 1995.

[55] Markou, G., Mourlas, Ch., Garcia, R., Pilakoutas, K., Papadrakakis, M., "Cyclic Nonlinear Modeling of Severely Damaged and Retrofitted Reinforced Concrete Structures", 7th ECCOMAS Thematic

Conference on Computational Methods in Structural Dynamics and Earthquake Engineering, COMPDYN 2019, Crete, Greece, 24–26 June 2019.

[56] Mourlas, C., Markou, G. and Papadrakakis, M. (2019), "Accurate and Computationally Efficient Nonlinear Static and Dynamic Analysis of Reinforced Concrete Structures Considering Damage Factors", Engineering Structures, 178 (2019), pp. 258–285.

[57] Gonzalez-Vidosa, F., Kotsovos, M.D. and Pavlovic, M. N. (1991), "A three-dimensional nonlinear finite-element model for structural concrete. Part 1: main features and objectivity study; and Part 2: generality study, Proceedings of the Institution of Civil Engineers, Part 2, Research and Theory", 91, pp. 517-544.

[58] Menegotto, M., and Pinto, P. E. (1973). "Method of analysis for cyclically loaded reinforced concrete plane frames including changes in geometry and non-elastic behavior of elements under combined normal force and bending." Proceedings, IABSE Symposium on Resistance and Ultimate Deformability of Structures Acted on by Well Defined Repeated Loads, Lisbon, Portugal, 15–22.

[59] Markou, G. and AlHamaydeh, M. (2017), "3D Finite Element Modeling of GFRP-Reinforced Concrete Deep Beams without Shear Reinforcement", International Journal of Computational Methods, International Journal of Computational Methods, 15(1), pp. 1-35.

[60] Martin, P., Fabio, T., Javier, M. R., Christis, Ch., Nicholas, K., Toula, O., Panayiotis, R., Panagiotis, K., Telemachos, P., Antonis, K. (2013), Seismic Retrofitting of RC Frames with Infilling (SERFIN Project), European Commission, Joint Research Center, Institute of the Protection and Security of Citizens.

[61] Holmes, W.T. (1996), "Policies and standards for reoccupancy repair of earthquake-damaged buildings", Earthquake Spectra, 10(3), pp. 197–208.

[62] Polese, M., Di Ludovico, M., Marcolini, M., Prota, A. and Manfredi, G., (2015), "Assessing repairability: simple tools for estimation of costs and performance loss of earthquake damaged reinforced concrete buildings", Earthquake Engineering in Structural Dynamics, 44(10), pp. 1539-1557.

[63] Markou, G., R. Sabouni, Suleiman, F. and El-Chouli, R. (2015), "Full-Scale Modeling of the Soil-Structure Interaction Problem Through the use of Hybrid Models (HYMOD)", International Journal of Current Engineering and Technology, 5 (2), pp. 885-892.

[64] Markou, G., AlHamaydeh, M. and Saadi, D., "Effects of the Soil-Structure-Interaction Phenomenon on RC Structures with Pile Foundations", 9th GRACM International Congress on Computational Mechanics, Chania, Greece, 4-6 June 2018, pp. 338-345.

[65] Mourlas, C., Gravett, D.Z., Markou, G., and Papadrakakis, M., "Investigation of the Soil Structure Interaction Effect on the Dynamic Behavior of Multistorey RC Buildings", VIII International Conference on Computational Methods for Coupled Problems in Science and Engineering, COUPLED PROBLEMS 2019, 3-5 June 2019, Sitges, Catalonia, Spain.

[66] Garcia, R., Jemaa, Y., Helal; Y., Guadagnini, M. and Pilakoutas, K. (2014), "Seismic Strengthening of Severely Damaged Beam-Column RC Joints Using CFRP", Journal of Composites for Construction, 18(2), 04013048.